공학석사 학위논문

Numerical Analysis of Projectile Impact on Concrete Structures Using LS-DYNA Software

LS-DYNA 프로그램을 이용한 콘크리트 구조물의 비상체 충돌에 관한 수치해석 연구

2018 년 2 월

서울대학교 대학원

건축학과

홍 준 기

공학석사 학위논문

Numerical Analysis of Projectile Impact on Concrete Structures Using LS-DYNA Software

LS-DYNA 프로그램을 이용한 콘크리트 구조물의 비상체 충돌에 관한 수치해석 연구

2018 년 2 월

서울대학교 대학원

건축학과

홍 준 기

Numerical Analysis of Projectile Impact on Concrete Structures Using LS-DYNA Software

지도 교수 강 현 구

이 논문을 공학석사 학위논문으로 제출함
2018 년 2 월

서울대학교 대학원
건축학과
홍 준 기

홍준기의 공학석사 학위논문을 인준함
2018 년 2 월

위 원 장 _____ (인)

부위원장 _____ (인)

위 원 _____ (인)

Abstract

Numerical Analysis of Projectile Impact on Concrete Structures Using LS-DYNA Software

Hong, Joon-Ki
Department of Architecture and Architectural Engineering
College of Engineering
Seoul National University

The concrete is a principal material that has been comprehensively used in the field of civil and architectural engineering including from high-rise structures to long-span bridges. Not only these typically representative buildings, but other structures and national major facilities such as nuclear power plants also have mainly adopted concrete in various ways. These concrete structures should be designed against severe accidents causing structural failure. In this regard, the structural safety of each concrete structure should be evaluated meticulously.

The primary purpose of this thesis is to suggest analytical methods to simulate the projectile impact on concrete target using the finite element software of ANSYS LS-DYNA. The analytical approach is suggested by establishing a numerical model in the software. It is used to simulate actual experiments in

the past, aircraft impact experiments conducted by Sandia National Laboratories in 1988, and imaginary blade impacts on an auxiliary building in the Nuclear Power Plants (NPPs).

The developed numerical analysis could reduce a huge amount of time and cost compared to actual experiments, without sacrificing accuracy. In addition, the constructed numerical model in the software predicted the test results effectively regardless of time, space, and size of the specimens. The suggested numerical methods for the projectile impact and local failure in this study are expected to be utilized in the diverse research fields on the design of national facilities or shelters and various analytical and experimental studies of projectile impact.

Keywords: aircraft impact, projectile impact, concrete structures, local failure, finite element analysis
Student Number: 2016-21093

Contents

List of Tables

List of Figures

List of Symbols

$a(t)$	acceleration of the projectile at each time, m/s^2
C_D	missile drag coefficient
c	viscous damping coefficient
d	diameter of the projectile, m
E_C	scabbing resistant energy, kN-m
E_{DC}	deformed energy of the concrete, kN-m
E_{DP}	deformed energy of the projectile, kN-m
E_K	kinetic energy of the concrete, kN-m
E_R	resistant energy of the concrete, kN-m
E_S	spalling resistant energy, kN-m
E_{steel}	modulus of elasticity of the steel, GPa
E_T	tunneling resistant energy, kN-m
$F(t)$	impact force at each time, kN
f_c'	compressive strength of the concrete, MPa

f_D	damping resisting force
f_r	tensile strength of the concrete, MPa
f_S	elastic resisting force
h_p	limit thickness of perforation, m
$h_{p,calc}$	perforation limit thickness calculated by empirical equations, m
h_s	limit thickness of scabbing, m
$h_{s,calc}$	scabbing limit thickness calculated by empirical equations, m
I_h	non-dimensional impact factor
K	reinforcement influence factor
k	lateral stiffness of system
M	mass of the projectile, kg
m	mass of the single degree of freedom
$m(t)$	mass at each time, kg
N	nose shape factor
$P_c(t)$	crushing force at each time, kN
$p(t)$	external force
S	dynamic increase factor

u	displacement of the mass
$\dot{u}$	velocity of the mass
$\ddot{u}$	acceleration of the mass
V_h^{open}	3-second peak gust wind speed, m/s
V_{min}	minimum velocity of projectile, m/s
v	velocity of the projectile, m/s
$v(t)$	velocity of the projectile at each time, m/s
x	depth of penetration, mm
α	effective mass coefficient
α_p	reduction factor for perforation failure
α_s	reduction factor for scabbing failure
α_w	water surface exposure coefficient
μ	mass distribution along with the length of the projectile, kg/m
ρ_{air}	air density, kg/m^3

Chapter 1. Introduction

1.1 Introduction

Concrete is a material that has been comprehensively utilized in civil and architectural construction of from high-rise structures to long-span bridges. Diverse development methods also have been studied actively. As various concrete structures provide people with a living space, these let the people more feel comfortable and help them to avoid the danger of accident from the external environment. Not only these typical buildings and bridges, but other structures such as government major facilities also mainly adopt concrete materials in various ways.

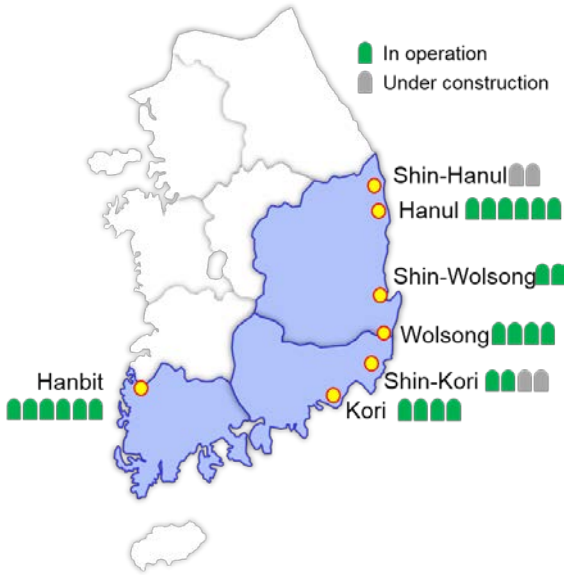

Figure 1-1 Location of Nuclear Power Plants in Korea

One of the main concrete national facilities in Korea is nuclear containment structures. As seen in **Figure 1-1**, the number of Nuclear Power Plant (NPP) in Korea is 24 units in 2016. It means that Korea is the 6th country in terms of

the largest number of the NPPs in the world. Today, 22 units are continuously operated in Korea.

Nuclear energy is generally regarded as one of the most realistic sources of energy since it can be produced regardless of weather conditions. The primary aim of the containment structures in Nuclear Power Plants (NPPs), playing a crucial role as final protection, is to prevent leakages of radiations caused by a wide variety of accidents, which is plausible even though it seems like more improbable under the normal situations. At the end, it can prevent people from being exposed to radioactive materials. In this regard, the safety issues in Nuclear Power Plants (NPPs) are entailed and should be observed by diverse codes meticulously and constantly.

In the past, there were mainly three calamitous accidents about NPPs inspiring people until nowadays. It was Three Mile Island (TMI) accident in 1979, Chernobyl accident in 1986, and Fukushima accident in 2011. Before the TMI accident, the construction of NPPs had been done merely focusing on the abilities of safety systems to prohibit design based accidents. After the accidents, there was an advance in comprehension of severe cases leading to a meltdown. From these cases, a lesson has been learned such that radiation leakages caused by accidents in NPP would need significant recovery time and costs. Interests on structural capacity of the NPPs have highly increased.

Figure 1-2 Aircraft Attacks on World Trade Center in 2001

Not only a kind of aforementioned severe accidents but also the assessment about impact situations have been stringently regarded in NPPs since the most disastrous scene in 2001. As shown in **Figure 1-2**, World Trade Center (WTC), the building deemed as an emblem of U.S., was collapsed by the impact of hijacked aircrafts. After this horrible terror, numerous research has been widely studied to guarantee the structural capacity against the impact accidents on NPPs. Even though it rarely seems to be directly correlated with NPPs, the U.S. Nuclear Regulatory Commission (NRC) classified the impact incidents as a beyond design basis event (BDBE) (NEI, 2011; Lee et al., 2013a).

Researchers could recognize the importance of the aircraft accidents from the 911 attack. Moreover the importance of structural redundancy for an earthquake has been emphasized again since the Tohoku disaster in 2011. In this way, regulations related to NPPs have been enhanced based on variable extreme loadings beyond the design criteria obtained from actual accidents although it has an extremely low probability to happen. To secure safety, the previous incidents have been reflected in the development and revision of regulations. The information obtained from manifold accident cases has been utilized as acceptance criteria of the regulations. As a result, it has been employed in existing or newly constructed containments. It has significantly contributed to the improvement of safety for nuclear containment structures (Moon and Choi, 2014). Not only the aircraft impact cases but also a wide variety of projectile impacts on concrete target are urgently necessary to be researched in the field of protection engineering and/or military industry. Variable studies relevant to the projectile impacts will continuously be conducted.

1.2 Objective and Scope

The primary purpose of this thesis is to suggest analytical methods to simulate the projectile impact on a concrete target using the finite element software, ANSYS LS-DYNA. Moreover, there is a need to verify previously suggested methods with the assumption of a concrete target including concrete containment structures and various concrete structural walls. The analytical approach is suggested establishing a numerical model in the software to simulate the actual experiments about aircraft impact conducted by Sandia National Laboratories in 1988. The reliability of the approach is evaluated by comparing the simulated results with the experimental results.

In addition, the blade impact on an auxiliary building in NPPs is also addressed in this thesis. Wind turbine blades could be fractured due to severe accidents causing the fragment impact on the exterior wall of the concrete auxiliary building. The aim of this analysis is to conduct the structural evaluation of the auxiliary building using LS-DYNA. The selected representative walls are used to examine the effects of the projectile impact depending on various thicknesses. The analytical approach is also conducted based on the existing local failure evaluation equations, which have been developed by previous researchers and research institutes. Along with the comparison of the analysis results with the test results, the existing local failure equations are used to verify the reliability of the numerical results.

Numerical analysis can reduce time and cost instead of conducting actual experiments. In addition, numerical modeling using software can predict the test results efficiently regardless of time, space, or size of the specimens. The suggested numerical methods about the projectile impact and local failure through this study are expected to be utilized in the diverse research fields due to not only increasing demand on national facilities or shelters but also needs regarding projectile impact research.

1.3 Organization of Thesis

This thesis consists of 6 chapters with 2 appendixes. The mainly concerned topics in each chapter are succinctly summarized as follows:

Chapter 1 addresses the background information about why the severe incidents should be considered in the design of national facilities. Especially, the impact on concrete target is the most prominent issue in the field. With respect to the specific issue, the primary aim and the scope of this study are summarized briefly. Based on the described contents in this chapter, this thesis is composed of the following chapters.

Chapter 2 describes considerable previous studies pertaining to the main objective of this thesis. This chapter is mainly comprised of two categories: aircraft impact and projectile impact on the concrete target with local failure of the concrete. Each subsection deals with chronologically diverse studies about previous experiments, evaluation strategies including empirical formulae, and numerical simulations at each classification.

Chapter 3 discusses modeling features of the finite element software, ANSYS LS-DYNA. The information about various numerical models implemented in the program, the hourglass control, and contact algorithms are explained in this chapter. The addressed keywords in this chapter are mostly adopted in the diverse analysis that the author performed previously. Moreover, these keywords are essentially employed to use in other simulations regardless of the type of the analysis.

Chapter 4 deals with the numerical analysis about the aircraft impact on the concrete wall according to the actual experiment performed by Sandia National Laboratories (SNL) in 1988. The representative aircraft model was F-4D jet, and is fully composed of countless particles by the Smoothed Particle Hydrodynamics (SPH) method. All data shows good agreement with the test results including the mass distribution of the aircraft, impact and

impulse, velocity, and displacement which were obtained from the actual experiment. Particularly, the acquired data on impact force and impulse is compared to the indirect method proposed by Riera (1968). Furthermore, the pertinent value about the essential coefficient is investigated again through the analysis.

Chapter 5 articulates about the blade impact analysis. This chapter mentions the background of this numerical analysis. A concrete auxiliary structure in an NPP is established in LS-DYNA. In the ocean in front of the NPP, several wind turbines are located and distant from the concrete structure with 1 kilometer. The main purpose of the analysis is to conduct the effects of the blade impact on the concrete structure caused by unforeseen accidents with blade fragments crashing into the structure. The implemented keywords are described in this chapter.

Chapter 6 summarizes all of the noteworthy perspectives and conclusions drawn from the aforementioned chapters. Furthermore, it is insisted that the covered contents in this thesis can be practical for the design of related industrial and building structures in various ways.

Lastly, **Appendixes A and B** are attached after the list of **References** in order to provide the ANSYS LS-DYNA keywords about the analyses mentioned in **Chapters 4 and 5**. The detailed information introduced in the keyword files is not provided since it has a lot of words to be presented in these two appendixes; thus, only the essential keywords are provided. It can be beneficial to other researchers who are interested in the numerical analysis on the concrete subjected to diverse impact loading.

Chapter 2. Review of Previous Studies

2.1 Background Theory

2.1.1 Basic Principles of Dynamics

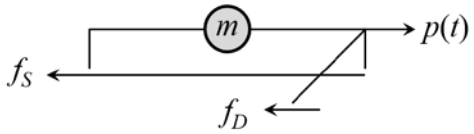

Figure 2-1 External Forces on Mass

In case of single degree of freedom systems, most equations of dynamics are determined in terms of the motion of the particles as a lumped mass, *m*. As shown in **Figure 2-1** when diverse forces are applied on a mass, the equation of motion due to the external force, $p(t)$, can be defined by displacement of the mass, $u(t)$, as shown in **Eq. (2-1)** and **Eq. (2-2)**, since it is varied along with time.

$$p - f_S - f_D = m\ddot{u} \tag{2-1}$$

where p is the external force, f_S means the elastic resisting force, f_D is the damping resisting force, m is the mass of the system, and $\ddot{u}$ indicates the acceleration of the mass.

$$m\ddot{u} + c\dot{u} + ku = p(t) \tag{2-2}$$

where m means the mass, $\ddot{u}$ is the acceleration of the mass, c is the viscous damping coefficient, $\dot{u}$ is the velocity of the mass, k is the lateral stiffness of the system, u is the displacement of the mass, and $p(t)$ means the external force in terms of time.

Initial conditions to find the solution of **Eq. (2-2)** are typically such that both initial displacement and initial velocity are zero as defined in **Eq. (2-3)**.

$$u(0) = 0 \qquad \dot{u}(0) = 0 \tag{2-3}$$

If $p(t)$ is assumed as a series of pulses during the extremely short period, the responses of the system can be determined as sum of responses at individual pulses.

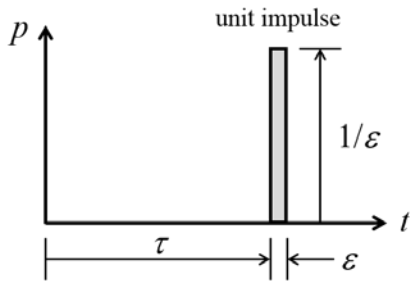

Figure 2-2 Unit Impulse

Figure (2-2) illustrates the unit impulse, $p(t) = 1/\varepsilon$, beginning at $t = \tau$ for ε seconds. Since the magnitude of the impulse is defined by integral with respect to time and is always constant at unity, the magnitude of the impulse during the time of ε is determined as $1/\varepsilon$.

The momentum is defined as mass times specific velocity. According to Newton's second law of motion, the rate of change of the momentum with respect to time is equal to the force (p) acting on the mass (m) as defined in **Eq. (2-4)**.

$$\frac{d}{dt}\left(m\dot{u}\right) \tag{2-4}$$

If the mass is constant, **Eq. (2-5)** is equal to the following:

$$p = m\ddot{u} \tag{2-5}$$

In other words, the momentum indicates the mass moving with the specific velocity. The external force (p) acting on the mass (m) induces the change of the momentum. If **Eq. (2-5)** is integrated by time, the impulse is defined as **Eq. (2-6)**.

$$\int_{t_1}^{t_2} p dt = m\left(\dot{u}_2 - \dot{u}_1\right) = m\triangle\dot{u} \tag{2-6}$$

The left side is the magnitude of the impulse and the right side indicates momentum which is mass times velocity. Therefore, **Eq. (2-6)** indicates that the impulse is equal to the change of the momentum.

2.2 Aircraft Impact

2.2.1 F-4D Jet Impact Experiment (Sugano et al., 1993c)

In 1988, a full scale F-4 Phantom impact test was conducted by Sandia National Laboratories (SNL) using their own facilities. One of the primary objectives of this experiment is to solve the questions that previous theoretical approaches left. It is also to determine an array of the responses to the aircraft considering uncertainties not involved in previous methods. Lastly, to make relatively accurate predictions of impact force is the other aim of this experiment. The Sandia National Laboratories (SNL) had a facility which was 600 m long two rocket rail. The representative F-4 Phantom, which had a weight of 469 tons at a speed of 215 m/s, crashed into a rigid reinforced concrete block. Some equipment in the F-4D model was removed to be carried on the rail, while sleds and rockets were attached. For instance, seats, gears, and flaps at the main wings were removed, whereas sled and rockets were added. As a result, the total impact weight of the aircraft was 19 tons.

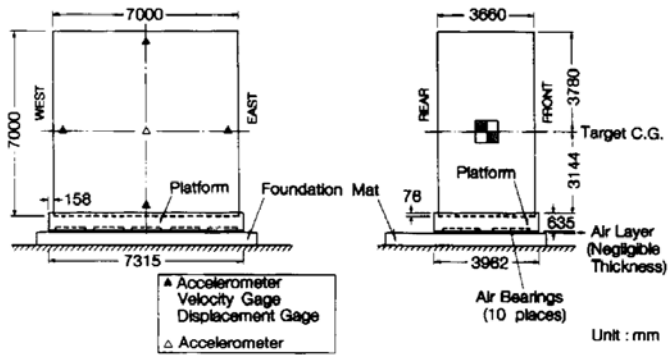

Figure 2-3 Layout of Reinforced Concrete Target

As seen in **Figure 2-3**, the massive reinforced concrete target had 7 m of height and width, and 3.66 m of thickness. The weight of the target was 469 tons, approximately 25 times of the F-4D aircraft. Through five instrumentations, the impact responses of the target were recorded including velocity, acceleration, and displacements. Major test results were described in the published paper (Sugano et al., 1993c).

Figure 2-4 F-4D Jet Impact on Concrete Target (Sugano et al., 1993c)

Figure 2-4 depicts the procedure of the aircraft impact. From the experiment, it was confirmed that the damage caused by the aircraft impact was not critical for the concrete target. It was speculated that the most of the energy was used to move the target rather than causing significant damage on the target. Considering these perspectives, an additional experiment was conducted (Sugano et al., 1993a and 1993b). Furthermore, the accuracy of

Riera function was verified, showing reliable results in the event of impact accidents. In addition, it was defined that the acceptable effective coefficient for mass is 0.9 through the experiment. What it means is that 10% of the projectile mass would be reduced during the impact. Finally, it was concluded that the impact area of the structure subjected to impact load can be measured as approximately twice the fuselage area.

2.2.2 Force-Time History Analysis

International Atomic Energy Agency (IAEA) specifies that one of the illustrated three evaluation methodologies, which are the energy balance, Force-Time History Analysis (FTHA), and Missile-Target Interaction Analysis (MTIA), should be used to evaluate damage caused by crash analytically (IAEA, 2003; Jiang and Chorzepa, 2014). Among these methods, the Force-Time History Analysis (FTHA) and Missile-Target Interaction Analysis (MTIA) are generally adopted for evaluation.

First, the FTHA method is performed adopting force-time history to figure out the behavior of structures. According to IAEA safety standards series (IAEA, 2003), force-time histories are determined from missile peculiarities or several assumptions of the solid target. Applying these histories accounts for conservative results to assess structural redundancy. It is because the effective load is diminutive considering the target flexibility (IAEA, 2003).

The typical method for force-time history analysis is the Riera function. Riera (1968) suggested an equation to calculate impact force on a target. This function has been widely used in research because of ease to evaluate the impact force of crushing projectiles. The basic principle of the Riera method is to calculate the impact force-time history based on the crushing strength of aircraft and conservation principles which are derived from the kinematic theorem (Lee et al., 2013b). First of all, impact force, $F(t)$, can be derived by differentiating the momentum equation as shown in **Eq. (2-7)**.

$$F(t) = \frac{d}{dt}\left[m(t)v(t)\right] \tag{2-7}$$

where $m(t)$ is mass and $v(t)$ is velocity at each time. Then,

$$F(t) = m(t)\frac{d}{dt}v(t) + v(t)\frac{d}{dt}m(t) \tag{2-8}$$

where $m(t)$ is mass and $v(t)$ is velocity at each time. **Eq. (2-8)** consists of inertia force induced by variation of velocity and force to reduce the mass of collision cross section (Lee et al., 2013b). Especially, the second term of **Eq. (2-8)** could be deleted in that as the rigid wall is assumed, deformation induced by impact force might be small so that almost mass could remain. Consequently, **Eq. (2-8)** can be simply revised as the below equation, **Eq. (2-9)**, since derivative of the velocity, $v(t)$, is equal to acceleration at each time, $a(t)$.

$$F(t) = m(t) \cdot a(t) \tag{2-9}$$

where $v(t)$ indicates velocity and $a(t)$ is acceleration at each time. However, the second term of **Eq. (2-8)** has to be considered in the aircraft impact analysis (Sugano et al., 1993c). In addition, a crushing force of cross section of the aircraft is equal to the inertia force of undestroyed parts of the aircraft. Therefore, **Eq. (2-10)** could be defined as the crushing force, $P_c(t)$ (Lee et al., 2013b).

$$P_c(t) = m(t)\frac{d}{dt}v(t) \tag{2-10}$$

where $m(t)$ is mass and $v(t)$ is velocity at each time. Meanwhile, derivative of mass with respect to time can be expressed in terms of mass per unit length and velocity as **Eq. (2-11)**.

$$\frac{d}{dt}m(t) = \mu\left[x(t)\right]v(t) \tag{2-11}$$

where μ indicates the mass distribution along with the impacted length (x) of the aircraft, $x(t)$ is the impacted length at each time, and $v(t)$ means velocity at each time. By substituting **Eq. (2-10)** and **Eq. (2-11)** into **Eq. (2-8)**, the impact force of an aircraft can be derived as **Eq. (2-12)** in accordance with the Riera function.

$$F(t) = P_c(t) + \mu\left[x(t)\right]v(t)^2 \tag{2-12}$$

where P_c(t) is crushing force, and μ means the mass distribution along with the impacted length (x) of the aircraft. Kar (1979) adopted and revised the Riera function including the effective mass coefficient, which should be defined through the real impact experiment. Kar (1979) suggested the effective mass coefficient (α) as the below equation which means that entire mass would not be affected during the crush in reality. In this regard, the loss of mass at impact is involved and **Eq. (2-12)** can be manipulated as below.

$$F(t) = P_c(t) + \alpha\mu\left[x(t)\right]v(t)^2 \tag{2-13}$$

where P_c(t) is crushing force, α is the effective mass coefficient, μ is the mass distribution along with the impacted length (x) of the aircraft. **Eq. (2-13)** is described in NEI 07-13 (2009) which has the guidelines for evaluation of aircraft impact (Seo and Noh, 2013). The value of an effective mass coefficient (α) should be defined based on the experiment results. From the previous full-scale experiment (Sugano et al., 1993c), it was turned out that 0.9 is appropriate for the effective mass coefficient. It means that when an aircraft impact on the target, the projectile loses 10% of its mass during the impact. In this way, the effective mass coefficient (α) is merely determined from the results of the actual experiments.

The essential advantage of FTHA is that the consideration of impact effects is relatively easy through dynamic time history analysis using an indirect method such as the Riera equation. However, typical drawbacks of the indirect method include that it has several limits. For instance, several assumptions should be postulated for the use of the Riera approach because it is a kind of indirect approach. First, target elements on which the aircraft would impact is rigid and flat. Second, the Riera formula is based on the perpendicular impact coinciding with the progressive axial destruction of the aircraft. Third, the uncrushed area is continuously moved with deccelerated velocity, while deconstructed regions are neglected. Also, the deformation only occurs in the vicinity of the rigid target. Lastly, the material characteristics of the aircraft is rigid and perfectly plastic (NEI, 2009; Fang and Wu, 2017). It also neglects secondary effects that might occur in realistic aircraft impact. It was figured out that there is a discrepancy between the analysis and reality (Jiang and Chorzepa, 2014). To supplement the aforementioned disadvantages and assumptions, the use of Missile-Target Interaction Analysis (MTIA) has been raised.

2.2.3 Missile-Target Interaction Analysis

Missile-Target Interaction Analysis (MTIA) is a method using the finite element analysis. Using the MTIA, users can perform diverse analyses explicitly with a model combined with targets and projectiles (IAEA, 2003). This method has been referred to consider variable circumstances which are significantly difficult to be conducted in actual tests. An amount of studies have been on the rise with explicit analysis using computational analysis programs including AUTODYN, ABAQUS, and ANSYS LS-DYNA. Combinations of targets and crushing projectiles are established in the diverse programs to observe a wide variety of structural nonlinear performances. The impact process can be activated by the defined initial velocity of the projectile.

For this direct method, it is aimed to find additional effects which are not

coincided in the indirect methods. One of the most advantages of using the MTIA is that the calculation of crushing area of the aircraft is not required. It is possible to consider the secondary effects such as fragments. Relatively accurate mass distribution should be required. To secure reliability, the results should be verified comparing with the specific results obtained from the Riera approach.

2.2.3.1 Wilt et al. (2011)

Wilt et al. (2011) conducted numerical simulations about the F-4D Phantom and F-15E aircraft. Two numerical methods were described to conduct analysis about the F-4D Phantom crash experiment. First of all, the method used a concrete model with the load history given from the experiment. Since the detail of the reinforcement layout was not illustrated in the paper (2001), the concrete density was modified instead of construction of a numerical model of reinforcements, commensurating with the actual mass of the experiment. Second, the time history data derived from the Riera method was introduced on the concrete model in the LS-DYNA analysis. The performed analyses show relatively accurate results compared to those obtained from the test. It is indicated that the described approach can predict performances of the targets.

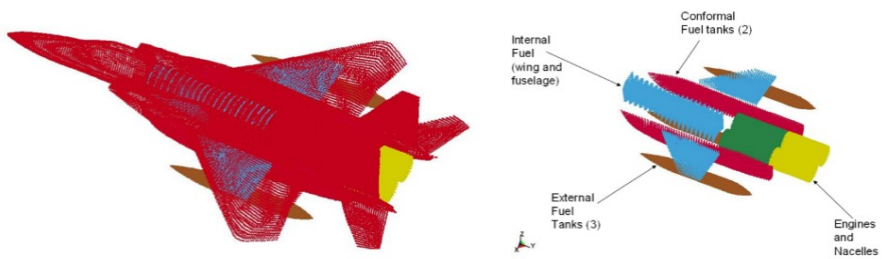

Figure 2-5 F-15E Model using SPH Method (Wilt et al., 2011)

The F-15E aircraft impact simulation was conducted using Smoothed Particle Hydrodynamics (SPH) method implemented in ANSYS LS-DYNA as shown

in **Figure 2-5**. The procedures to import the F-15E model were as follows: First, TrueGrid was employed to generate the external surface mesh of the aircraft. Then, the external figure was changed into IGES file. Finally, this format was changed into elements constructed using the SPH method in ANSYS LS-DYNA.

One of the remarkable features of this study is that diverse material properties were used to establish the more accurate numerical model of the F-15E aircraft including internal fuel, fuel tanks, and engines. The external mesh made of countless SPH particles was separated into several parts. Each part had 1 m length along the longest direction. To match with appropriate mass contributions, FORTRAN was used to set pertinent mass distributions automatically. Aluminum and steel were used in the SPH parts as the external skin of the aircraft and the engines, respectively. As material keywords, MAT_PLASTIC_KINEMATIC model was used for the skin and the engines, while the fuel was constructed using MAT_NULL model as a liquid. To compare the accuracy of the analytical results based upon the initial velocity, the numerical analysis was performed with respect to the low speed (112 m/s) and the high speed (190 m/s). As a result, each result showed lower impact force by about 33% and 4%, respectively. This indicates that the Riera method gives more conservative results in the impact force.

An additional simulation about the impact on reinforced concrete building was performed. Concrete damage model (MAT_072) in the finite element program was applied to the concrete, while MAT_003 was used for reinforcement steel. It was revealed that response of the concrete subjected to impact forces can be predicted using LS-DYNA and be affected by the engine attached to aircraft.

2.2.3.2 Arros and Doumbalski (2007)

As seen in **Figure 2-6**, numerical analysis about aircraft impact on imaginary

containment building was performed utilizing ANSYS LS-DYNA. The fictitious containment building had 158 ft of width and 118 ft in length, and 98 ft was given as the height of the structure.

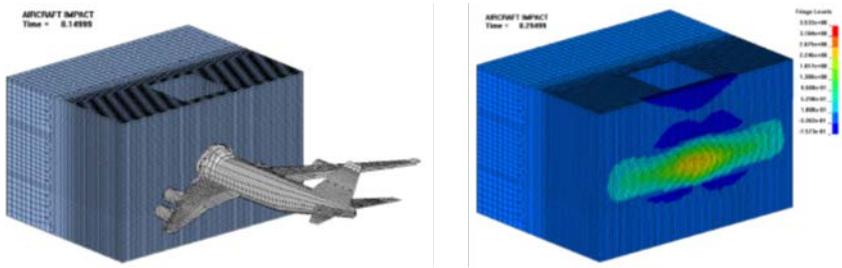

Figure 2-6 Aircraft Impact Analysis (Arros and Doumbalski, 2007)

Considerable minute mesh was constructed in the front wall where the aircraft crashed into, while rear side of the structure contained coarse mesh. The Winfrith (MAT_084) was adopted as a concrete model. Properties including the concrete strength and yield stress of reinforcements were set to pertinent values as usual.

Different methods were used to conduct impact simulation. The first method was to input idealized force curve based on the Riera force history. The other method was the missile-target interaction analysis (MTIA). Boeing 747-400 was employed depicting genuine dimensions and geometry in the software. The constructed model was simplified in terms of the number of elements. The mass and impact force distribution was adapted to be commensurate with the results drawn from the Riera approach.

From this research, it is concluded that the results of the analysis contained high-frequency factors with respect to the behavior of the structure compared to the results from using the Riera function. Compared to the results derived from the MTIA, the maximum displacement at the impact point was almost close to each other, but loading area should be modified for the Riera analysis. Lastly, nonlinear analysis would be more acceptable since it could reduce high frequency responses compared with linear analysis.

2.2.3.3 Seo and Noh (2013)

Seo and Noh (2013) performed B767 aircraft impact on a containment structure. There was an assumption that the targeted containment structure is reinforced by steel fibers. The reason why the steel fibers were considered is that steel fiber reinforced concrete (SFRC) shows high performance in terms of tensile strength or flexural strength as the dosage rate of steel fibers increases. SFRC can be used to prevent from severe accidents. The introduced study (Seo and Noh, 2013) aimed to evaluate impact resistance of the containment structure compared with normal reinforced concrete without steel fibers.

The representative containment model was the OPR-1000, which is the name of Korean standard nuclear power plant. It consists of a hemispherical dome on the top of the building, cylindrical wall, and foundation slab. The OPR-1000 uses the Pressurized Water Reactor (PWR) method, while the CANDU employs the Pressurized Heavy Water Reactor (PHWR) method. Most of the concrete structures in Korea have adopted PWR method except for only 4 units (Hong and Kang, 2016).

For material properties, the strength of the SFRC was determined based on the previous study about the expected strength model. The fiber content varied along 0.0%, 0.5%, 1.0%, and 1.5%. As for reinforcements, 420 MPa of yield strength and 0.3 of Poisson's ratio were applied as material properties. Plastic Kinematic Model (MAT_003) was accepted with Constrained Lagrange in Solid keyword (CLIS). The main purpose of using CLIS keyword is to combine steel reinforcement to the concrete target.

The liner elements were specified using the Piecewise Linear Plasticity Model (MAT_00#) with Contact Automatic Surface to Surface Tiebreak as a contact algorithm. Dynamic Increase Factor (DIF) was multiplied to the strength of materials according to ACI 349-17. The DIF of 1.25, 1.10, 1.29 were applied respectively.

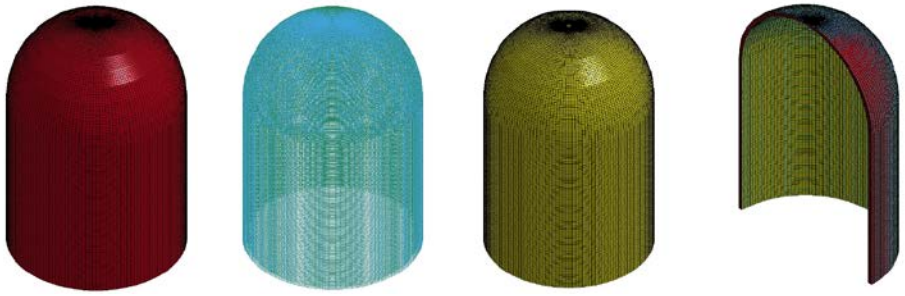

Figure 2-7 Constructed Containment Model (Seo and Noh, 2013)

Figure 2-7 shows establihsed containment building in ANSYS LS-DYNA. B767 was a hijacked airplane crashing into the World Trade Center in the U.S. in 2001. The velocity of the airplane was set to 150 m/s. The impacted area of the B767 was assumed as twice the area of the fuselage according to Riera (1968) and Sugano et al. (1993). Even though the actual impacted area varies during the impact, the varied impacted area in this study was assumed as changed similarly to the fuselage area. The location of the impact was perpendicular to the middle of the cylindrical wall since it is a considerably critical assumption when the maximum bending moment effect occurs (Seo and Noh, 2013).

As the fiber content increased from 0.0% to 1.5%, the eroded area of the concrete reduced because SFRC made the concrete durable by increasing the compressive strength and improving the resistance for the impact. In all of the 4 cases, steel liner was not deteriorated and the rear side opposite to the impact point showed no effects during the impact.

2.2.3.4 Lee et al. (2013a, 2014)

Lee et al. (2013a) performed impact simulations on a prestressed concrete containment building using both LS-DYNA and AUTODYN. Boeing 747 was adopted as a representative numerical model in the analysis. In this study, the mass distribution and weight were determined according to the reported model by OECD/NEA (2002). The effective mass coefficient was determined

to be 0.9 which was validated from the experiment by Sugano et al. (1993c). The effects of the target shape, the prestressing force, different impact points, and the incidence angle of the crashing airplane were considered in this study.

In aspects of the target shape, the results for the impact on spherical shape showed the impulse and momentum of almost 80% for the impact on the rectangular shape. It indicates that the impact force would be reduced by 12.5% for the spherical type. It was because the ends of the wings of the aircraft were not contacted with the target in the case of the spherical shape.

To discover different performances according to the tendon prestressing effects, 0 ton, 50 ton, 100 ton, 500 ton, and 1000 ton were applied to the containment model. It was figured out that tendon effects caused the increase on the overall stiffness of the containment structures. However, the impact force was not affected by the presence of the prestressing force. It means that the prestressing force can only lead to a decrease of the local failure since impact force is mainly involved by the shape of the target.

About the effects of the incidence angle of the aircraft, Lee et al. (2013a) figured out that the angle perpendicular to the wall was a critical case among the 15 degree, 30 degree, and 45 degree. For impact position, four positions were adopted from bottom of the wall to the top of the dome. At each incident position, the aircraft collided with the wall perpendicularly. At the end of analyses, it was concluded that the position where the aircraft crashed into is not an influential factor affecting impact force or impulse.

Lee et al. (2014) additionally conducted a computational analysis considering the F-4D crash experiment and verified the validity for Missile-Target Interaction Analysis (MTIA) using ANSYS LS-DYNA. The CSCM Concrete Model (MAT_159) was employed for a concrete material, while material number 3 was for reinforcement steel. Impact simulation was conducted using different aircraft models, which were Lagrangian model, Smoothed Particle

Hydrodynamics (SPH), and Hybrid model. The Hybrid model employs the mixed Lagrangian and SPH elements. The liquid fuel was considered in the analysis.

According to Lee et al. (2014), **Eq. (2-13)** can be simplified as a function that consists of only velocity and mass distribution with the effective mass coefficient (α) of 1.0. It can be expressed as in **Eq. (2-14)** considering the results of the analysis, because the ratio of the crushing force of the aircraft impact force is less than the variation in change of the effective mass coefficient factor (α = 1.0 and α = 0.9).

$$F(t) \cong \mu\left[x(t)\right]v(t)^2 \tag{2-14}$$

where μ represents the mass distribution along with the impacted length (x) of the aircraft, $x(t)$ is the impacted length at each time, and $v(t)$ indicates velocity at each time.

2.3 Projectile Impact on Concrete Target

From the F-4D jet impact on the concrete wall (Sugano et al., 1993c), 20 mm of the penetrated depth was recorded at the region of the concrete target where the aircraft crashed into. The region impacted by aircraft engine showed the maximum penetration depth of 60 mm (Sugano et al, 1993c). It explains that during the aircraft impact, local failure cannot be affected by fuselage since it has relatively large impact area rather than the engine. On the other hand, the engine accounts for significant influence on the local failure of the concrete. Considering these noteworthy conclusions, the further experiment was conducted, which was about the assessment of local failure due to replica engine impact on the targets (Sugano et al., 1993a and 1993b). The additional experiment is covered in **Section 2.2.2** as one of the previous studies on the local failure of the concrete.

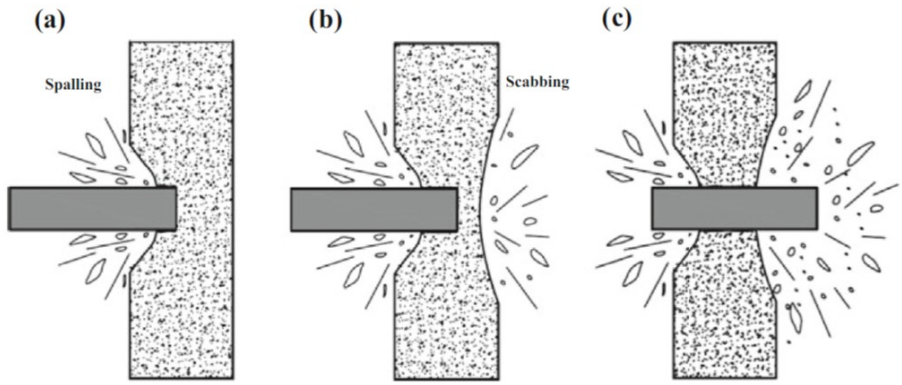

Figure 2-8 Effects of Projectile Impact on Concrete Target (Li et al., 2005)
(a) Penetration; (b) Scabbing; (c) Perforation

In this regard, the local failure should be considered meticulously in the evaluation. The form of the local failure is mainly classified into three types (Kennedy, 1976; Li et al., 2005; Fang and Wu, 2017): (1) penetration, (2) scabbing, and (3) perforation as illustrated in **Figure 2-8**. First of all, the penetration is the failure of the front region of the concrete panel causing

spalling which is adjacent fragment at the impact face due to the impact. However, there are no failures including cracks at the rear face. The scabbing involves simultaneously concrete debris at rear face with the penetration depth at front side. The debris at rear side is generally similar in size to concrete cover, which is outside the reinforcement. Lastly, the perforation means the situation that a projectile fully penetrates through the concrete target. In this case, the projectile has residual velocity. The primarily interested four parameters to evaluate the local failure caused by missiles are the penetration depth (x), the limit thicknesses of scabbing (h_s) and perforation (h_p), and the minimum velocity of the projectile (v_{min}) (Li et al., 2005; Fang and Wu, 2017).

To evaluate the local failure, actual experiments, empirical formulae, and numerical methods are mainly considered as methodologies. Experimental data is always the best way to comprehend responses of the concrete panel. Test results grant extensive view on understanding about the local failure and are regarded as the significant reference to validate empirical or numerical methods in terms of reliability. The most important method in the local failure is empirical approaches based on the experimental results. The empirical methods have been generally drawn from the experimental data which were manipulated by the curve fitting (Li et al., 2005). This is the reason why the empirical models are partially limited according to the parametric ranges from the test (Fang and Wu, 2017). Numerical methodology using computational tools, meanwhile, maybe more efficient and reliable than other approaches with respect to time and cost.

2.3.1 Previous Experimental Studies

2.3.1.1 Kojima (1991)

Kojima (1991) conducted a number of missile impact tests of concrete slab with manifold conditions in 1987 and 1988. The primary objective of this experiment was to gain diverse local behavior of the concrete slab. The thickness, the speed of the projectile, missile hardness, rear steel lining, and multi-layered concrete slab were regarded as variations in the experiment.

Table 2-1 Test Specimens (Kojima, 1991)

Specimen	Target		Missile	
	Type	Thickness (cm)	Velocity (m/s)	Type
R-24-X	Single	24	200	Hard
R-18-X	Single	18	200	Hard
R-12-X	Single	12	200	Hard
R-12-Y	Single	12	150	Hard
R-12-Z	Single	12	100	Hard
R-18-S	Single	18	200	Soft
R-12-S	Single	12	200	Soft
W-09-X	Double	9+9	200	Hard
W-12-X	Double	6+12	200	Hard
W-12-S	Double	6+12	200	Soft
L-18-X	Liner	18	200	Hard
L-12-X	Liner	12	200	Hard

Table 2-1 summarizes the list of specimens. The name of constructed specimens consists of three terms. The first term expresses the type of the target. ‘Single’ means one layer of the concrete slab, while ‘double’ describes two layers. ‘Liner’ indicates the concrete slab with steel liner at the rear side. The second term addresses the thickness of the target. In this experiment, five types in terms of thickness were used. Lastly, the third term means the

projectile velocity. ‘X’, ‘Y’, and ‘Z’ indicate 200 m/s, 150 m/s, and 100 m/s, respectively. These definitions were for only hard type of the projectile. For soft type, the velocity was always 200 m/s and defined as ‘S’.

Table 2-2 Material Properties for Specimens (Kojima, 1991)

		Compressive Strength (MPa)	Cracking Strength (MPa)	Yield Strength (MPa)	Tensile Strength (MPa)
Concrete		27	3.3	-	-
Rebar (SD35)	D6	-	-	389.3	540
	D10	-	-	420	570
	D13	-	-	384	530
Steel Liner (SS41)				Not accurate	432.5

Table 2-2 summarizes material properties used in the experiment. For missiles, hard-nosed and soft-nosed types were employed with 2 kg of the weight for both types. One of these characteristics is the soft-nosed missile contained about 140 mm long hollow area with 2 mm of the thickness. As for measurements, the projectile speed, the response of the target, reaction force, and the strain of the reinforcements and steel liner were measured through the pertinent methods. Among the five measurements, the velocity of the projectile was not measured by the instrument. Instead, the distance between the missile and the target was divided by the reaching time to calculate the speed of the missile.

According to the results, the damage and the penetration depth were decreased as the thickness of the target was thickened. However, the size of the spalling which was observed at the front size was enlarged since the spalling of concrete cover happened much easily. Given the same thickness, the double layered concrete target showed the similar impact resistance compared to the single layered target for the soft missile, but lower resistance was monitored

for the hard missile.

2.3.1.2 Sugano et al. (1993a; 1993b)

From the full-scale jet impact experiment (Sugano et al., 1993c) performed by Sandia National Laboratories (SNL), the bigger penetration depth was observed at the region where aircraft engine crashed into rather than the region where the main body was impacted. In this way, it gave significant insight that the local failure appeared in the concrete target was mainly caused by extra components of the aircraft such as engine or wings. In other word, the engine occupies considerable weight on the local failure of the concrete. Based on the noteworthy outcomes, the additional experiment was designed and the results were summarized by Sugano et al. (1993a; 1993b).

The mainly concerned subject of this experiment was to figure out the local failure of the concrete target subjected to the deformable engine impact. The test consisted of small scale, intermediate scale, and full scale specimens. For both small scale and intermediate scale experiment, a wide variety of parameters were considered to determine the different responses of the target. The initial speed of the engine was significantly different for these tests, but 215 m/s was maintained for the full scale test. The size of the concrete target was also varied. 1.5 m, 2.5 m, and 7 m were kept for the small scale, intermediate scale, and full scale, respectively.

To predict the local damage of the concrete panel, several empirical equations were selected. Chang, CEA-EDF, Degen, and CRIEPI formulae were decided for the perforation limit thickness. Meanwhile, Chang, CRIEPI, and Bechtel equations were chosen to predict the scabbing limit thickness. These determined equations are known for the accuracy of its reliability.

Based on the results of the further experiment, two factors were introduced to the existing equations: the reduction factor α_p and α_s for perforation and scabbing. Finally, it was concluded that 0.65 of α_p and 0.6 of α_s were more

appropriate value for the reduction factors in terms of conservative aspects (Sugano et al., 1993b).

2.3.1.3 Kang et al. (2016)

Kang et al. (2016) performed the experimental study to figure out the performance of Ultra-High Performance Concrete (UHPC) panel subjected to the impact load. The target compressive strength of the panels was 180 MPa. The thicknesses of the concrete panels were designated as 10 mm, 20 mm, and 30 mm. The process to make UHPC followed K-UHPC method by Korea Institute of Civil Engineering and Building Technology (KICT). The projectile was designed similar to the kinetic energy of bullets. The projectile used in this experiment had 20 mm of the diameter, 32 g of the weight, and 180 m/s of the velocity.

As a result, all of the specimens with 10 mm of the thickness showed perforation failure. It involved clear failure at the front surface with 332 mm^2 of the punched area on average and the scabbing failure. The average punched area was similar to the sectional area of the projectile with the diameter of 20 mm. For other thicknesses, above the thickness of 20 mm, the perforation failure was not appeared, but for 30mm thickness, the spalling was only observed. In general, the panels made by UHPC showed outstanding impact resistance. In particular, the scabbing failure of the concrete panel was associated with the shear failure due to the shear plug effect, causing diagonal shear failure at the impact point.

2.3.2 Empirical Methodology for Local Failure

In this section, a wide variety of equations to predict local failure of the concrete targets are listed. The primary concerned terms organizing equations are penetration depth (x), perforation limit depth (h_p), scabbing limit depth (h_s), mass of the projectile (M), diameter of the projectile (d), unconfined compressive strength of concrete (f_c'), and impacting velocity of the projectile (v).

2.3.2.1 Petry (1910)

A wide variety of equations to predict local failure of the concrete structures have been developed by military studies and experimental data. Among these various studies, Petry equation is the oldest model (Petry, 1910). Since Petry (1910) developed his own available equation in 1910, diverse researches on the evaluation of the impact capacity of concrete structures have been actively conducted. For Petry equation, local failure is determined using the equation of motion for partial region, which is based upon the research on hard missile impact on the concrete structures. For penetration depth (x) in Petry formula,

$$\frac{x}{d} = K\left(\frac{M}{d^3}\right)\log_{10}\left(1+\frac{v^2}{19974}\right) \tag{2-15}$$

where K is the reinforcement influence factor, M is mass of the projectile, d is diameter of the projectile and v is the initial velocity of the projectile. The term K in **Eq. (2-15)**, the reinforcement influence factor, is dependent on the concrete types. For instance, k value is given to 0.000636, 0.000339, and 0.000226 for massive concrete, normal reinforced concrete, and specially reinforced concrete (Li et al., 2005). Based on this formula, Amirikian (1950) proposed an improved equation which can determine the perforation and scabbing limit depth simply. For perforation limit depth (h_p) and scabbing limit depth (h_s),

$$h_p = 2.0x \tag{2-16}$$

$$h_s = 2.2x \tag{2-17}$$

where x is the penetration depth.

2.3.2.2 Ballistic Research Laboratory (BRL) (1941)

For the calculation of the penetration depth caused by a solid projectile, the equation was proposed by Ballistic Research Laboratory (BRL) in 1941 (Li et al., 2005).

$$\frac{x}{d} = \frac{1.33 \times 10^{-3}}{\sqrt{f_c'}} \left(\frac{M}{d^3} \right) d^{0.2} v^{1.33} \tag{2-18}$$

where M is mass of the projectile, d is the diameter of the projectile and v is the initial velocity of the projectile. Based on this equation for the penetration depth, Chelapati et al. (1972) and Linderman et al. (1973) developed the equation (Fang and Wu, 2017). The perforation limit depth (h_p) and scabbing limit depth (h_s) were given by:

$$h_p = 1.3x \tag{2-19}$$

$$h_s = 2.0x \tag{2-20}$$

where x is penetration depth.

2.3.2.3 Army Corp of Engineers (ACE) (1943)

Army Corp of Engineers (ACE) and BRL obtained extensive data from experimental results. As a result, ACE offered an equation for the penetration depth (x) in statistical ways as below:

$$\frac{x}{d} = \frac{3.5\times10^{-4}}{\sqrt{f_c'}}\left(\frac{M}{d^3}\right)d^{0.215}v^{1.5} + 0.5 \tag{2-21}$$

where d is the diameter of the projectile, f_c' is the compressive strength of the concrete target, M is mass of the projectile and v indicates the initial velocity of the projectile. The missile caliber density corresponds to the term m/d^3 in **Eq. (2-21)** (Li et al., 2005). From this equation, perforation limit depth (h_p) and scabbing limit depth (h_s) can be derived as follows:

$$\frac{h_p}{d} = 1.32 + 1.24\left(\frac{x}{d}\right) \tag{2-22}$$

$$\frac{h_s}{d} = 2.12 + 1.36\left(\frac{x}{d}\right) \tag{2-23}$$

where x means penetration depth and d is diameter of the projectile. The perforation limit depth (h_p) is applicable to the range between 1.35 and 13.5 for x/d. For scabbing limit depth (h_s), the range of x/d is from 0.65 to 11.75. If the range of the h_s/d and h_p/d is smaller than 3, the results are regarded as in the conservative range.

2.3.2.4 Modified National Defense Research Committee (NDRC) (1946)

National Defense Research Committee (NDRC) performed further experiments based on the equation proposed by ACE. Finally, NDRC suggested the modified NDRC equation.

$$\frac{x}{d} = 2G^{0.5} \quad (G \le 1) \tag{2-24}$$

$$\frac{x}{d} = G + 1 \quad (G > 1) \tag{2-25}$$

$$G = 3.8 \times 10^{-5} \frac{NM}{d\sqrt{f_c'}} \left(\frac{v}{d} \right)^{1.8} \quad (2\text{-}26)$$

where N is the nose shape factor, M is mass of the projectile, d is the diameter of the projectile, f_c' is the compressive strength of the concrete target, and v is the initial velocity of the projectile. The term N varies based on the type of the nose shape of the projectile. In general, there are four types to use this equation; flat nose, blunt nose, spherical nose, and very sharp nose. The values for each type are 0.72, 0.84, 1.0, and 1.14.

$$\frac{h_p}{d} = 3.19 \left(\frac{x}{d} \right) - 0.718 \left(\frac{x}{d} \right)^2 \quad (2\text{-}27)$$

$$\frac{h_s}{d} = 7.91 \left(\frac{x}{d} \right) - 5.06 \left(\frac{x}{d} \right)^2 \quad (2\text{-}28)$$

where x indicates the penetration depth and d means the diameter of the projectile. The most advantageous characteristic of the modified NDRC equation is it can be used in diverse cases with comparatively accurate results since this equation is based on the theoretical concept. The modified NDRC equation is referred to in NEI 07-13 (2009) which is one of the most representative guidelines for evaluations of the aircraft impact.

2.3.2.5 Bechtel (1974)

Bechtel Power Corporation (Silter, 1980) suggested an equation for scabbing limit depth (h_s) considering the missile impact on nuclear containment structures as below (Li et al., 2005). This equation is applicable to the rigid projectiles.

$$\frac{h_s}{d} = 38.98\left(\frac{M^{0.4}v^{0.5}}{f_c'^{0.5}d^{1.2}}\right) \tag{2-29}$$

where M is mass of the projectile, v is the initial velocity of the projectile, f_c' is the compressive strength of the concrete target, and d is diameter of the projectile.

2.3.2.6 Degen (1980)

Degen (1980) proposed equation for perforation limit depth (h_p) improved from the Modified NDRC equation. The term x/d is equal to the same suggested in the Modified NDRC equation.

$$\frac{h_p}{d} = 2.2\left(\frac{x}{d}\right) - 0.3\left(\frac{x}{d}\right)^2 \quad (x/d \le 1.52) \tag{2-30}$$

$$\frac{h_p}{d} = 0.36 + 1.29\left(\frac{x}{d}\right) \quad (1.52 \le x/d \le 13.42) \tag{2-31}$$

where x indicates the penetration depth and d means the diameter of the projectile.

2.3.2.7 Chang (1981)

An equation for flat nose projectile was developed by Chang (1981). The perforation limit depth (h_p) and scabbing limit depth (h_s) were proposed as below:

$$\frac{h_p}{d} = \left(\frac{61}{v}\right)^{0.25}\left(\frac{Mv^2}{d^3 f_c'}\right)^{0.5} \tag{2-32}$$

$$\frac{h_s}{d} = 1.84\left(\frac{61}{v}\right)^{0.13}\left(\frac{Mv^2}{d^3 f_c'}\right)^{0.4} \quad (2\text{-}33)$$

where v is the initial velocity of the projectile, M is mass of the projectile, f_c' is the compressive strength of the concrete target, and d is the diameter of the projectile.

2.3.2.8 Modified Degen & Chang (1993)

The Sandia National Laboratories (SNL) performed the aircraft engine impact test to observe local failure of concrete targets (Sugano et al., 1993a; 1993b). The SNL found that evaluated value show differences between the Degen and the Chang formula due to the deformation of the projectile during impact. In this regard, Sugano et al. (1993a; 1993b) suggested the Modified Degen and Chang formula introducing the reduction factor α_p and α_s for perforation equation (Degen formula) and scabbing equation (Chang formula) respectively.

In the report (Sugano et al, 1993b), the reduction factor (α_p) for the Degen equation was determined as 0.65 considering conservative aspects even though 0.6 is more reliable value. Therefore, the Degen equation for perforation limit depth (h_p) were multiplied by 0.65 of the determined reduction factor as expressed in **Eq. (2-34)** and **Eq. (2-35)**.

$$\frac{h_p}{d} = 0.65\left[2.2\left(\frac{x}{d}\right) - 0.3\left(\frac{x}{d}\right)^2\right] \quad (x/d < 1.52) \quad (2\text{-}34)$$

$$\frac{h_p}{d} = 0.65\left[0.36 + 1.29\left(\frac{x}{d}\right)\right] \quad (1.52 \le x/d \le 13.42) \quad (2\text{-}35)$$

where x means the penetration depth and d represents the diameter of the projectile. On the other hand, the reduction factor (α_s) for the Chang equation

was seen to between 0.55 and 0.65. As a result, the reduction factor for scabbing limit depth were figured out that 0.6 was appropriate conservatively. In this way, 0.6 was introduced into the Chang equation for scabbing limit depth (h_s) as described in below.

$$\frac{h_s}{d} = 0.6\left[1.84\left(\frac{61}{v}\right)^{0.13}\left(\frac{Mv^2}{d^3 f_c'}\right)^{0.4}\right] \tag{2-36}$$

where v indicates the initial velocity of the projectile, M is mass of the projectile, d describes the diameter of the projectile, and f_c' means the compressive strength of the concrete target.

2.3.2.9 Hughes (1984)

Aforementioned equations are derived from date obtained from various impact experiments with light weight and rigid projectile. After that, numerous prediction equations considering impact of middle weight and low speed such as turbine or tornado projectile have been proposed. Among these equations, the Hughes's formula is renowned (Chung et al., 2010). The equation proposed by Hughes considers effects of the tensile strength of the concrete using Dynamic Increase Factor (DIF) (Kim et al., 2017).

For perforation limit depth (h_p)

$$\frac{h_p}{d} = 3.6\left(\frac{x}{d}\right) \quad (x/d < 0.7) \tag{2-37}$$

$$\frac{h_p}{d} = 1.58\left(\frac{x}{d}\right) + 1.4 \quad (x/d \geq 0.7) \tag{2-38}$$

For scabbing limit depth (h_s),

$$\frac{h_s}{d} = 5.0\left(\frac{x}{d}\right) \quad (x/d < 0.7) \tag{2-39}$$

$$\frac{h_s}{d} = 1.74\left(\frac{x}{d}\right) + 2.3 \quad (x/d \geq 0.7) \tag{2-40}$$

$$\frac{x}{d} = 0.19\frac{NI_h}{S} \tag{2-41}$$

where x is penetration depth, d means the diameter of the projectile, N is the nose shape of the projectile, I_h is non-dimensional impact factor, and S represents dynamic increase factor. The term N, the nose shape of the projectile, is given to 1.0 for flat type, 1.12 for blunt type, 1.26 for spherical type, and 1.39 for very sharp type. The definition of I_h in **Eq. (2-42)** is non-dimensional impact factor (Li et al., 2005) and expressed by

$$I_h = \frac{Mv^2}{d^3 f_r} \tag{2-42}$$

where M is mass of the projectile, v is the initial velocity of the projectile, d is diameter of the projectile and f_r is the tensile strength of the concrete target. Moreover, as shown in **Eq. (2-43)**, Dynamic Increase Factor (DIF) S was introduced in the Hughes's formula to account for the effects of the strain rate on the tensile strength of the concrete (Li et al., 2005).

$$S = 1 + 12.3\ln\left(1 + 0.03I_h\right) \tag{2-43}$$

where I_h indicates non-dimensional impact factor. The major difference between the Modified NDRC formula and the Hughes formula in terms of the nose shape factor is that the nose shape factor in the Hughes equation determines flat nose as a criterion, while spherical type is the basis in the Modified NDRC formula.

2.3.2.10 CRIEPI (1991)

The Central Research Institute of Electric Power Industry (CRIEPI) suggested

perforation and scabbing limit depth as shown in **Eq. (2-44)** and **Eq. (2-45)**.

$$\frac{h_p}{d} = 0.6\left(\frac{61}{v}\right)^{0.25}\left(\frac{Mv^2}{d^3 f_c'}\right)^{0.5} \tag{2-44}$$

$$\frac{h_s}{d} = 1.75\left(\frac{61}{v}\right)^{0.13}\left(\frac{Mv^2}{d^3 f_c'}\right)^{0.4} \tag{2-45}$$

where v indicates the initial velocity of the projectile, M is mass of the projectile, d describes the diameter of the projectile, and f_c' means the compressive strength of the concrete target. The reference velocity is equal to 61 m/s, and the CRIEPI formula is converted from the Chang formula.

2.3.2.11 Energy Penetration Method (2017)

Hwang et al. (2017) proposed new formula to predict diverse modes for the local failure of concrete targets. The suggested formula is called as the energy-based penetration model as shown in **Figure 2-9**.

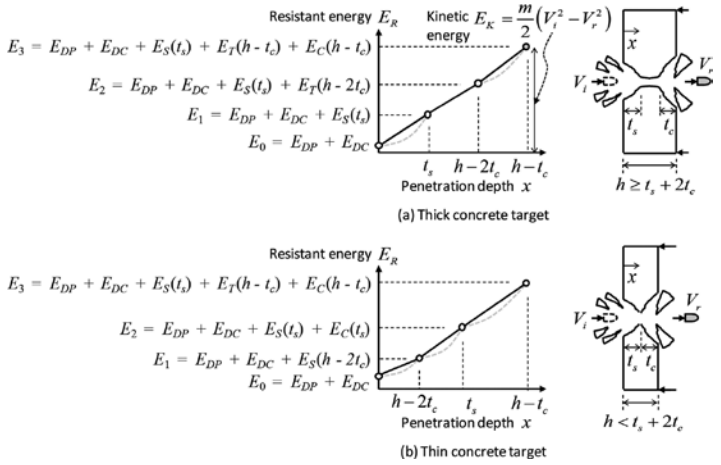

Figure 2-9 Concept of Energy-Based Penetration Model (Hwang et al., 2017)

The notable asset of the suggested energy-based penetration model is the

penetration depth and residual velocity can be determined conveniently depending on the energy conservation law (Hwang et al., 2017). The energy-based penetration model can predict penetration depth using the relationship between kinetic energy (E_K) and the resistant energy (E_R) of the concrete. For instance, the penetration will occur when the ratio of the kinetic energy compared to the resistant energy exceeds unity ($E_K / E_R > 1$). On the other hand, if the ratio E_K/E_R is smaller than unity ($E_K / E_R < 1$), the penetration will not be happened.

The resistant energy of the concrete is composed of five terms as shown in **Eq. (2-46)**. Especially, the resistant energy contains three failure modes, which are spalling, tunneling, and scabbing failure (Hwang et al., 2017).

$$E_R = E_{DP} + E_{DC} + E_S + E_T + E_C \tag{2-46}$$

where E_{DP} is the deformed energy of the projectile, E_{DC} indicates the deformed energy of the concrete, E_S means the spalling resistant energy, E_T is the tunneling resistant energy, and E_C is the scabbing resistant energy.

For verification of the reliability of the proposed model, previous studies were included to be compared with the results drawn from the energy-based penetration model. 414 specimens were adopted with various the target thicknesses, the concrete strength, the concrete density, the diameter of the projectiles, the initial velocity of the projectiles, and reinforcing ratio. As a result, it was concluded that the results derived from the proposed energy-based penetration model showed good agreement with existing experimental results.

Table 2-3 listed in the next page summarizes all of the proposed empirical equations addressed in this chapter briefly.

Table 2-3 Proposed Equations for Local Failure

Equation	Perforation Limit Depth (h_p)	Scabbing Limit Depth (h_s)	Penetration Depth (x)
ACE	For $(1.35 \le x/d \le 13.5)$ $\frac{h_p}{d} = 1.32 + 1.24\left(\frac{x}{d}\right)$	For $(0.65 \le x/d \le 11.75)$ $\frac{h_s}{d} = 2.12 + 1.36\left(\frac{x}{d}\right)$	$\frac{x}{d} = \frac{1.33\times10^{-3}}{\sqrt{f_c'}}\left(\frac{M}{d^3}\right)d^{0.2}v^{1.33}$
Bechtel		$\frac{h_s}{d} = 38.98\left(\frac{M^{0.4}v^{0.5}}{f_c'^{0.5}d^{1.2}}\right)$	
BRL	$h_p = 1.3x$	$h_s = 2.0x$	$\frac{x}{d} = \frac{3.5\times10^{-4}}{\sqrt{f_c'}}\left(\frac{M}{d^3}\right)d^{0.215}v^{1.5} + 0.5$
Chang	$\frac{h_p}{d} = \left(\frac{61}{v}\right)^{0.25}\left(\frac{Mv^2}{d^3 f_c'}\right)^{0.5}$	$\frac{h_s}{d} = 1.84\left(\frac{61}{v}\right)^{0.13}\left(\frac{Mv^2}{d^3 f_c'}\right)^{0.4}$	
CRIEPI	$\frac{h_p}{d} = 0.6\left(\frac{61}{v}\right)^{0.25}\left(\frac{Mv^2}{d^3 f_c'}\right)^{0.5}$	$\frac{h_s}{d} = 1.75\left(\frac{61}{v}\right)^{0.13}\left(\frac{Mv^2}{d^3 f_c'}\right)^{0.4}$	
Degen	For $x/d < 1.52$, $\frac{h_p}{d} = 2.2\left(\frac{x}{d}\right) - 0.3\left(\frac{x}{d}\right)^2$ For $1.52 \le x/d \le 13.42$, $\frac{h_p}{d} = 0.36 + 1.29\left(\frac{x}{d}\right)$		x/d is equal to Modified NDRC formula.

Hughes	$\frac{h_p}{d}=3.6\left(\frac{x}{d}\right)\quad (x/d<0.7)$ $\frac{h_p}{d}=1.58\left(\frac{x}{d}\right)+1.4\ (x/d\geq 0.7)$	$\frac{h_s}{d}=5.0\left(\frac{x}{d}\right)\quad (x/d<0.7)$ $\frac{h_s}{d}=1.74\left(\frac{x}{d}\right)+2.3\ (x/d\geq 0.7)$	$\frac{x}{d}=0.19\frac{NI_h}{S},\ I_h=\frac{Mv^2}{d^3 f_r}$ $S=1+12.3\ln(1+0.03I_h)$
Modified Degen & Chang	For $x/d<1.52$, $\frac{h_p}{d}=0.65\left[2.2\left(\frac{x}{d}\right)-0.3\left(\frac{x}{d}\right)^2\right]$ For $1.52\leq x/d\leq 13.42$, $\frac{h_p}{d}=0.65\left[0.36+1.29\left(\frac{x}{d}\right)\right]$	$\frac{h_s}{d}=0.6\left[1.84\left(\frac{61}{v}\right)^{0.13}\left(\frac{Mv^2}{d^3 f_c'}\right)^{0.4}\right]$	
Modified NDRC	$\frac{h_p}{d}=3.19\left(\frac{x}{d}\right)-0.718\left(\frac{x}{d}\right)^2$	$\frac{h_s}{d}=7.91\left(\frac{x}{d}\right)-5.06\left(\frac{x}{d}\right)^2$	$\frac{x}{d}=2G^{0.5}\quad (G\leq 1),\ \frac{x}{d}=G+1\quad (G>1)$ $G=3.8\times 10^{-5}\frac{NM}{d\sqrt{f_c'}}\left(\frac{v}{d}\right)^{1.8}$ *N*: Nose Shape Factor Flat (0.72), Blunt (0.84), Spherical (1.0), Very Sharp (1.14)
Modified Petry	$h_p=2.0x$	$h_s=2.2x$	$\frac{x}{d}=K\left(\frac{M}{d^3}\right)\log_{10}\left(1+\frac{v^2}{19974}\right)$ *K*: Reinforcement influence factor 0.000636 (massive plain concrete), 0.000339 (normal reinforced concrete), 0.000226 (specially reinforced concrete)

2.4 Discussion

This chapter described an overview of a wide variety of previous studies about from experimental testing and theoretical approaches to recent numerical simulations. In particular, the subjects described in this thesis focus on the aircraft impact and the local impact on the concrete target.

Numerous experimental tests have been performed widely to figure out the impact performance of the concrete targets. Based on massive experimental results, diverse equations to evaluate local impact failure more conveniently have been developed since the modified Petry equation was proposed.

These equations contain several assumptions to measure impact effect on the concrete structures. The first assumption is that the projectile should impact on the concrete target perpendicular to the surface of the target. The proposed equations by prior researchers do not consider variations on the impact angle. These assumptions are made for conservative aspects. Based on the assumptions, the users can evaluate local failure more practically using simple calculations.

Also, studies on the numerical analysis of the impact have been previously performed. In particular, nuclear power plant components such as auxiliary buildings should be designed meticulously against impact based on the relevant design codes. In this regard, using finite element software, a series of missile target interaction analyses are conducted to evaluate the impact performance of the target. Additionally, existing empirical equations can be used to verify the analytical results and reliability.

Chapter 3. Modeling Features of Finite Element Software

The most critical advantage of using finite element analysis programs is that practical software can reduce substantial amount of time and cost. There are an array of Finite Element Analysis (FEA) tools to simulate diverse numerical analyses such as ABAQUS, AUTODYN, ANSYS LS-DYNA, ADINA, and DIANA. In particular, ANSYS LS-DYNA is specialized in and capable of performing nonlinear and 3 dimensional finite element analysis in the case of entailing large deformation such as the impact, crash, explosion, or collapse accidents.

ANSYS LS-DYNA provides users with a wide variety of concrete models with a specific number, for instance, Pseudo Tensor model (MAT_016), Concrete Damage Model (MAT_072R3), Winfrith Concrete model (MAT_084), Johnson Holmquist Concrete model (MAT_111), and Continuous Surface Cap Model for Concrete which is called CSCM model (MAT_159). Among these provided concrete models, Concrete Damage Model (Karagozian and Case Concrete), Winfrith Concrete, and Continuous Surface Cap Model for Concrete (CSCM) are widely utilized as a concrete model in LS-DYNA. Each concrete model implemented in the FEA program has diverse characteristics, and some models require additional keywords to illustrate concrete behavior as explained in the following sections.

3.1 Concrete Materials

3.1.1 Karagozian and Case Concrete Model (MAT_72R3)

The Concrete Damage Model (MAT_72R3) is usually called as Karagozian & Cases Concrete (KCC) model in the field. It is a three-invariant model using three shear failure surfaces (LSTC, 2016a). Three independent parameters consist of yield, maximum, and residual failure surfaces with a plasticity based formulation. These independent failure surfaces can alter their shape according to the hydrostatic pressure of the element. This concrete model has been adopted to obtain responses of the concrete from the standard uniaxial, biaxial, and triaxial tests in tension and compression.

The KCC model requires numerous parameters to simulate concrete behavior. To verify parameters, sufficient experiments need to be performed. However, the KCC model can automatically generate material properties based on the compressive strength in order to increase the convenient. The concrete density is also required in the case of the dynamic analysis (Schwer and Malvar, 2005). Therefore, users can easily utilize the KCC model by only inputting representative information including strength and density, remaining other information default.

However, the KCC model does not contain erosion and crack parameters like the CSCM model. In order to figure out erosion and crack mechanism, additional keyword, MAT_ADD_EROSION, should be implemented. It involves a wide variety of parameters related to failure of the concrete. The basic concept of this additional keyword is when the performance of the material satisfies the specific values the user introduced, the concrete elements are deleted (Vasudevan, 2012).

3.1.2 Winfrith Concrete Model (MAT_084)

The Winfrith concrete model was invented in 1980s and embedded into LS-DYNA in 1991. The purpose of this concrete model is to obtain variable responses of the concrete structures under impact loading and blast loading (Wu et al., 2012; Vasudevan, 2012). For the impact simulation, the Winfrith model displays relatively stiff behavior, while the KCC model and the CSCM model show more accurate outcomes.

The key advantage is that the number of mainly considered parameters (four) is relatively small and it is simpler to use than other models. Users specify the unconfined compression strength and tensile strength of concrete to utilize the Winfrith concrete model (Schwer, 2011). The users should execute an additional binary keyword to obtain the data of cracks such as widths, location, and direction, with greater accuracy.

3.1.3 CSCM Model (MAT_159)

The CSCM concrete model was developed for analysis about impact or blast. Its validations have been already done by a wide variety of studies (Seo and Noh, 2013). The CSCM concrete model has elastic-softening behavior steps for stress-strain relationship (Wu et al., 2012). It can demonstrate peak strength under no confinement. Also, post-peak softening and brittle ductile transition are illustrated, but with low accuracy. It has a tendency to be ductile in the event of pressure loading and little influenced by the effects of the strain rate. In addition it is stiff under blast, while good agreements can be derived for impact loading.

The compressive strength should be determined between 20 MPa and 58 MPa, while the maximum aggregate size should be set to between 8 mm and 32 mm. Based on the compressive strength, the stiffness, three-dimensional yield strength, hardening, and softening are determined. Meanwhile, the maximum size of the aggregate is needed only for the softening behavior of the damage

formulation (Murray et al., 2007).

The principal difference between other concrete models is the failure criteria that is implemented in the CSCM concrete model as ERODE card. It is a parameter that users can easily manage to model the failure of concrete. Erosion of the concrete is activated based on a determined erosion coefficient in this card. With respect to the erosion factor, unity means the erosion is independent of the strain, while the erosion coefficient is less than unity, the erosion of the concrete never take place (Remennikov and Kong, 2012). The erosion coefficient at zero also indicates no erosion effects. If the erosion value is greater than unity, the concrete elements will be failed once the strain reaches the maximum principal strain. For instance, 1.1 of the erosion coefficient means that the concrete elements have the maximum principal strain of 10%. Some elements which exceed the specified maximum principal strain will be deleted. In general, the erosion coefficient is determined between 5 and 10 percent of maximum principal strain (Murray et al., 2007). **Table 3-1** discusses the major features of the diverse concrete models according to the study by Wu et al. (2012).

Table 3-1 Characteristics of Concrete Models (Wu et al., 2012)

Simulation Cases	KCC Model (MAT_072R3)	Winfrith Model (MAT_084)	CSCM (MAT_159)
General Behavior	- Shear dilation behavior - Brittle ductile transition	- Perfect elastic-plastic stress-strain behavior for tension and compression - No shear dilation behavior - No brittle ductile transition - No softening in compression	- Elastic-softening behavior - Shear dilation behavior - Brittle ductile transition
Tri-axial Comp.	- Peak strength - Post-peak softening behavior - Brittle ductile transition	- Peak strength - Post-peak softening behavior for only tension - No brittle ductile transition	- No plateau point - Very ductile - High impact of the strain rate
Pressure	Without strain rate shows good results	With strain rate shows good results	Low effects of the strain rate and ductile behavior
Blast	Good	Stiff	Stiff
Impact	Good	Stiff	Good
Perforation	Yes	None	Yes

Among the three concrete models, the CSCM was utilized in this thesis since it was developed to determine the behavior of the concrete under impact and is easy to use with relatively accurate results.

3.2 Reinforcement Material

MAT_PLASTIC_KINEMATIC (MAT_003) is generally used to construct steel reinforcement in the structures. It is because the most advantage of using this model is cost effectiveness with an elastic plastic response and to simulate isotropic and kinematic hardening effects of the beam elements (Vasudevan, 2012). The hardening effect is implemented in this model using a tangent modulus (Johansson and Fredberg, 2015).

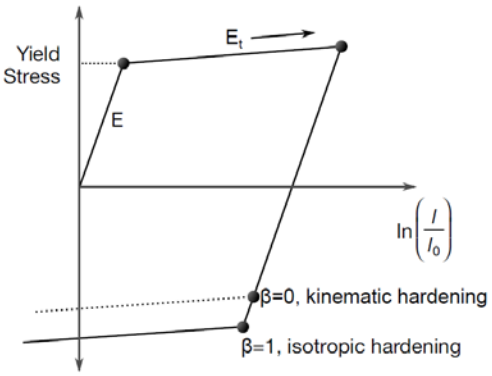

Figure 3-1 Hardening Effects for Plastic Kinematic Model (LSTC, 2016a)

Figure 3-1 illustrates hardening response for plastic kinematic model in the use. Based on the value of the beta, the hardening effects would be defined as kinematic (beta=0) or isotropic (beta=1).

Strain rate can be considered using the Cowper and Symonds model which implemented in material type 3. The introduced model is mainly considered in the case of blast simulation.

3.3 Hourglass Control

One-point integration is considerably used in numerical analysis considering cost efficiency because the fully integrated elements require substantial computational time to solve problems. However, one-point quadrature in

elements typically causes mesh instability with distortion regarded as the primary demerit of the method which is generally called as hourglassing (Belytschko et al., 1984). Therefore, one-point quadrature requires efforts to diminish hourglass effects in a various way.

Hourglass modes, which are nonphysical modes of deformation, can take place in all under-integrated elements such as solid elements producing no stress (Johansson and Fredberg, 2015). To minimize the hourglass effects, ANSYS LS-DYNA offers two forms of hourglass control which are viscous and stiffness formulations. Users can determine the types of the hourglass control specifying the type number. In general, Type 1 to Type 5 are widely adopted to control the hourglass effects. For instance, the numbers from 1 to 3 mean viscous formulation, while 4 and 5 indicate stiffness formulation.

Hourglass management can be activated using CONTROL keyword. The default option is set to Type 1, which indicates standard viscous hourglass control form. Type 2 and Type 3 are also one of the viscous formulations. Type 2 option is the Flanagan-Belytschko integration for solid elements, whereas Type 3 is the Flanagan-Belytschko with exact volume integration (LSTC, 2016a). The viscous formulations corresponding to the nodal velocity are generally used in the numerical analyses involving high strain rate such as explosion. Among the three stiffness hourglass control options, Type 1 is the cheapest formulation. The recommended coefficient value is usually less than 0.15.

Type 4 and Type 5 are the typical classifications in stiffness formulations. In particular, Type 4 and Type 5 are known as the Flanagan-Belytschko integration and the Flanagan-Belytschko with exact volume integration, respectively. The stiffness formulations proportionating to the nodal displacement should be determined between 0.1 and 0.03, though 0.03 is typically recommended. Other types of the hourglass control are generally employed in the special cases when the large aspect ratio is defined or the

assumed material is too much soft like foam or rubber. Therefore the aforementioned types are general and easy to manage the hourglass effects.

The relevant keywords to manage the hourglass effects are HOURGLASS, CONTROL_HOURGLASS, CONTROL_ENERGY, DATABASE_GLASTAT, DATABASE_MATSUM, and DATABASE_EXTENT_BINARY.

The HOURGLASS keyword is to control the hourglass effect for each part and should be defined in HGID card in PART keyword of the specific part. The CONTROL_HOURGLASS is to control global hourglass effects, but it is overwritten by the HOURGLASS keyword if the hourglass control for each part is defined using the HOURGLASS keyword. The hourglass energy for global or specific parts is calculated automatically once the HGEN card of CONTROL_ENERGY keyword is determined as 2. The HGEN card is the option to calculate the hourglass energy. HGEN = 1 indicates that the hourglass energy will not be calculated.

The DATABASE_GLASTAT keyword and DATABASE_MATSUM keyword are used to monitor the hourglass energy for global system and each part modeled in ANSYS LS-DYNA, respectively. Each hourglass energy can be observed through the PrePost by checking the status examined in matsum for individual materials or glastat for the overall system in the ASCII of the Post icon. If shell elements are established, DATABASE_EXTENT_BINARY keyword should be defined. In particular, SHGE card should be set to 2 in order to monitor the hourglass energy of the shell structures.

The most crucial fact is that the hourglass energy of both each material and entire system should be compared to the internal energy as a ratio between them. The hourglass energy for global system and specific parts should be less than 10 % of the internal energy to attain accurate results.

3.4 Method to Bond Concrete and Rebar

CONSTRAINED_LAGRANGIAN_IN_SOLID (CLIS) is greatly accepted to simulate reinforcements embedded in the concrete. Two approaches to combine reinforcements and the concrete are to share the common nodes or to use CLIS keyword (Johansson and Fredberg, 2015). Among numerous input blanks in the CLIS keyword, only a few input data is critically required to utilize this keyword. Most of all, reinforcement parts should be defined as a slave part, while concrete parts which containing reinforcements should be inserted in a master part. Johansson and Fredberg (2015) verified that there are no major discrepancies between sharing the nodes and using the CLIS keyword.

Chapter 4. Numerical Analysis of Aircraft Impact

4.1 Summary of Previous Experiment

In this chapter, F-4D jet impact analysis is performed according to the actual experiment by Sandia National Laboratories in 1988 (Sugano et al., 1993c). As described in **Chapter 2**, the main purpose of this experiment was to resolve doubts that previous theories contained and to inspect assorted performance when the aircraft impacts on the concrete target. Furthermore, it was possible to define various uncertainties not considered in previous theories. The other significant aim of this testing was to monitor impact force accurately.

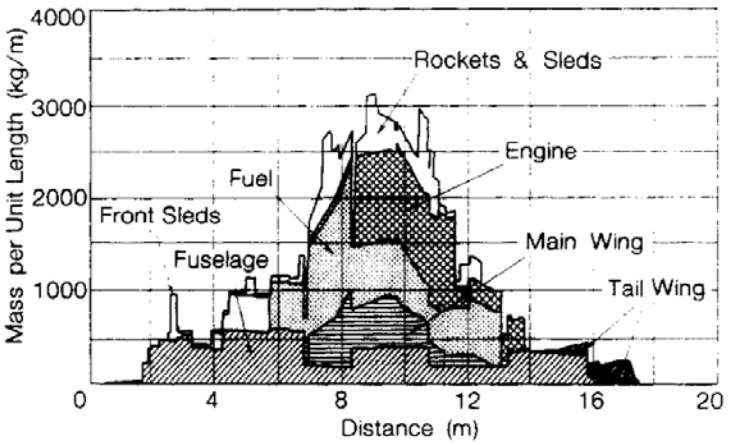

Figure 4-1 Mass Distribution of F-4D Jet in Experiment (Sugano et al., 1993c)

Figure 4-1 demonstrates the mass distribution of the F-4D jet accepted in this testing. Several apparatus were ignored, resulting in 19 tons of the impact weight of the F-4D aircraft. From this testing, it was concluded that Riera method, which is one of the most powerful approaches to figure out impact force, was substantially reliable. Moreover, 10% of the mass did not affect the

impact force, and the impact area was roughly double the fuselage impact area.

4.2 Numerical Model in LS-DYNA

The aircraft and the target constructed as a finite element would be directly crushed each other. It is a problem that the initial velocity should be assumed for dynamic analysis (NEI, 2009). Through this direct method, it is aimed to find additional effects which are not coincided in the indirect method. One of the most advantageous characteristics of using the MTIA is no need to calculate crushing area of the aircraft. Additionally it is possible to consider secondary effects such as fragment. However, considerably exact mass distribution is required to be introduced since the reliability of results drawn from the analysis is dependent on the accuracy of the introduced mass distribution compared to the test. To secure accurate results, it should be verified between the results obtained from the analysis as the direct method and the Riera approach as the indirect method.

4.2.1 F-4D Jet Modeling

As for traditional finite element analysis, manifold meshes were constructed to connect elements to nodes. When it came to analytical cases with large deformation, there were troubles with resolving considerable mesh distortion. To solve these difficulties, mesh-free methodology was used as a substitute of the conventional way. The typical approach of mesh-free methods is Smoothed Particle Hydrodynamics (SPH) method (Wilt et al., 2011).

To establish the numerical model using the SPH method, two properties should be defined: physical properties and geometrical properties. First of all, the physical properties involve the mass, density, and constitutive laws. This information of the properties is addressed through ELEMENT_SPH keyword. The geometrical properties indicate the status of each particle when it is constructed in the software.

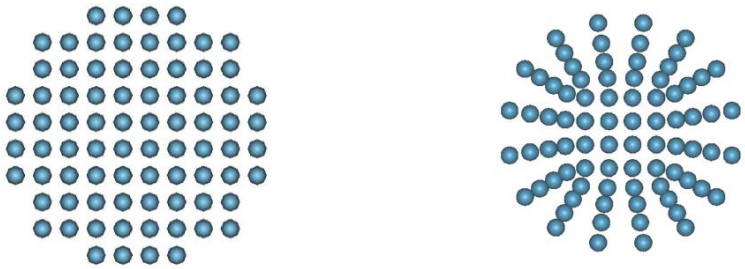

Mesh Type 1 Mesh Type 2

Figure 4-2 Types for Generated Mesh of SPH (LSTC, 2016b)

Figure 4-2 illustrates mesh types of the SPH method. The SPH mesh should be constructed, keeping regular consistencies as possible. In this regard, the type 1 of the meshes is better than the type 2 since the type 1 displays uniform distance between particles. Coupling finite elements and SPH elements were realized by using contact algorithms. Users can choose any NODES_TO_SURFACE contact keyword where the slave part is defined with SPH elements and the master part is defined with finite elements (LSTC, 2016b)

For F-4 Phantom, the Smoothed Particle Hydrodynamics (SPH) without any mesh was applied to consider large deformations during the impact. Due to disconnected particles between each other, the particles were spread out at impact. Therefore, it is possible to consider secondary effects of debris or fuel (Kostov et al., 2015). The 3 dimensional F-4D model was given as STL file. It is imported into LS-DYNA through the PrePost. The initial model is made of

shell elements for only the external shape, while the inside of the shell was empty. Instead, SPH particles were filled inside the shell using SPH generation function in ANSYS LS-DYNA. The distance between particles is mostly constant as the mesh type 1 in **Figure 4-2**.

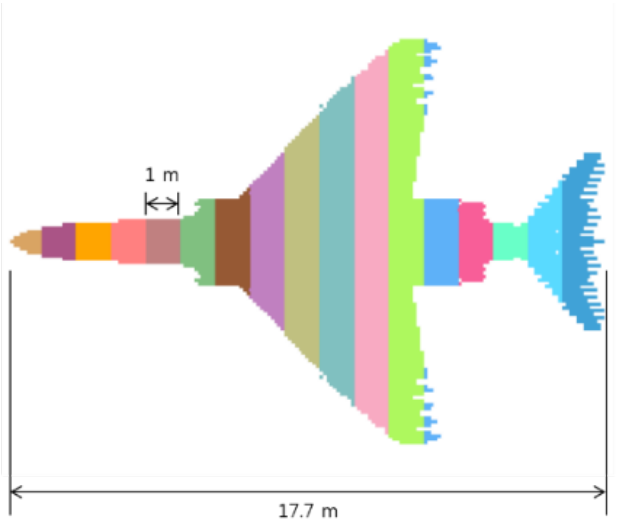

Figure 4-3 SPH Model for F-4D Jet

The basic concept in aircraft modeling in this study was that F-4 Phantom only consists of same materials with SPH elements. In other words, there are no classifications about various materials such as engine, fuel, or fuselage. Mass for each length was differentiated to combine multiple mass distribution of several parts. First of all, SPH elements were generated through LS-PrePost. As shown in **Figure 4-3**, it was divided into several parts along with the unit length (1 m) of the F-4 Phantom model to introduce mass information at each length.

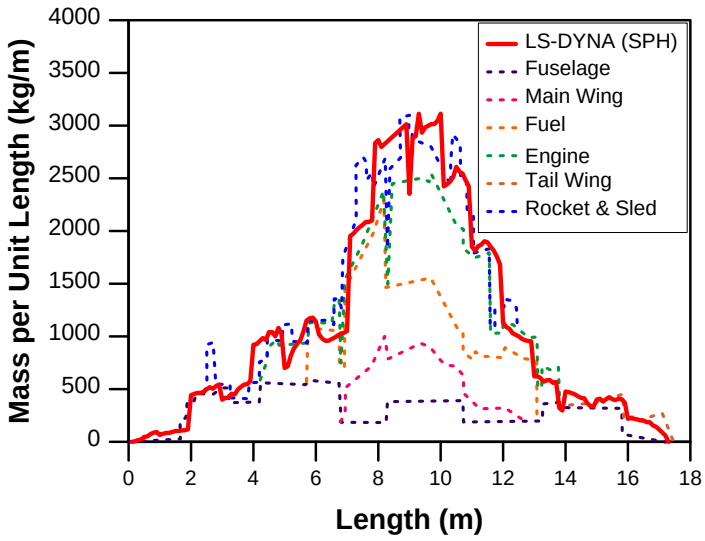

Figure 4-4 Mass Distribution Comparison with Test

To match with the mass distribution for an actual test illustrated in **Figure 4-1**, numerous values for mass were determined at particles since each length had different number of SPH elements. The mass per unit length could be determined the number of elements multiplied by the introduced mass value. **Figure 4-4** represents the comparison of mass distribution between the experiment and analysis in this study, and illustrates commensurate outcomes in terms of the mass distribution compared to the actual test. Therefore, it can be concluded that the aircraft model constructed in ANSYS LS-DYNA is valid to conduct the impact simulation.

Aluminum was assumed as a material for the F-4D jet using plastic kinematic model (MAT_003) in ANSYS LS-DYNA as well as for the reinforcement model. The specific properties for the F-4D jet are summarized in **Table 4-1** (Wilt et al., 2011).

Table 4-1 Aircraft Element Properties (MAT_003)

	Density (kg/m^3)	Modulus of Elasticity (GPa)	Yield Stress (MPa)	Poisson's Ratio
Aluminum	2770	69	95	0.33

In this study, the failure strain (FS) of 1.8 was applied according to the results performed by Lee et al. (2014). Even though some inserted conditions are quite different from the previous study such as contact conditions, components, properties, it can be applied in this model as well.

4.2.2 Concrete Target

For concrete target, foundation mat and platform was neglected in this analysis in order to simplify the analysis conditions. A concrete block directly collided with the aircraft was merely established in ANSYS LS-DYNA. As a boundary condition, the target was assumed such that it can only move to the direction corresponding to the F-4D jet path crashing into the target. Therefore, restraint of the direction along which the aircraft would move was released.

As mentioned in **Chapter 3**, the ANSYS LS-DYNA provides several material types to establish concrete models. For instance, MAT_024 (Piecewise Linear Plasticity Model), MAT_072 (Karagozian and Case Concrete), MAT_084 (Winfrith Concrete), MAT_111 (Johnson-Holmquist Concrete), and MAT_159 (CSCM) are frequently used in analysis corresponding to the concrete material. To observe various characteristics for concrete models, the MAT_159 concrete material model was employed in this study since it requires basic information about concrete, for instance, the density, the compressive strength, and the aggregate size. It is easy to use for concrete modeling. Since there were no details about concrete, the compressive strength of the concrete was basically assumed as 30 MPa. The detailed properties for the CSCM concrete model are summarized in **Table 4-2**. The concrete block had 7 m of width and height, and depth with 3.66 m as perfectly same as the actual experiment. The size of the mesh was 0.07 m at each side.

Table 4-2 Concrete Material Properties (MAT_159)

	Density (kg/m^3)	ERODE	f_c' (MPa)	Maximum Aggregate Size (mm)
CSCM Concrete	2615	1.05	30	19

MAT_003 (PLASTIC_KINEMATIC) material model was widely employed as the reinforcement. It was generated as a truss element considering conservative aspect (Seo and Noh, 2013). If the reinforcements are constructed as a beam element, the behavior of the reinforcement can be underestimated due to the resistance to flexural behavior. The analysis time can be reduced using the truss element for reinforcement steel because reinforcement elements only resist axial deformation. As specific information about embedded reinforcements was not provided, D-13 steel was basically assumed in the analysis. The specific properties about MAT_003 in LS-DYNA are shown in **Table 4-3**.

Table 4-3 Reinforcement Material Properties (MAT_003)

	Density (kg/m^3)	E_{steel} (GPa)	Poisson's Ratio	Yield Stress (MPa)	Failure Strain
Reinforcement	7850	200	0.3	420	0.2

The CONSTRAINED_LAGRANGE_IN_SOLID keyword was used to simulate reinforcements embedded in the concrete by setting reinforcement steel as a slave part, while the concrete element as a master part.

4.2.3 Contact

Particles consisting of the F-4D model were defined using DEFINE_BOX keyword. Using this keyword, the particles located outside the specified box were not considered during the analysis. In this regard, it is possible to reduce computational cost. For impact condition between the SPH modeling and the

target, CONTACT_AUTOMATIC_NODE_TO_SURFACE keyword was applied. The aircraft SPH elements were defined as slave parts, whereas master parts were set to the concrete target including steel reinforcements. The velocity was 215 m/s using INITIAL_VELOCITY keyword, which can introduce part speed easily.

4.3 Analysis Results

The cardinal objective of using the Riera function is to calculate the impact force for aircrafts. At first, the impact force drawn from the Riera method was conducted based on the given mass distribution condition. As Lee et al. suggested (2014), **Eq. (2-14)** neglecting crushing force was employed. As a result, **Figure 4-5** was derived.

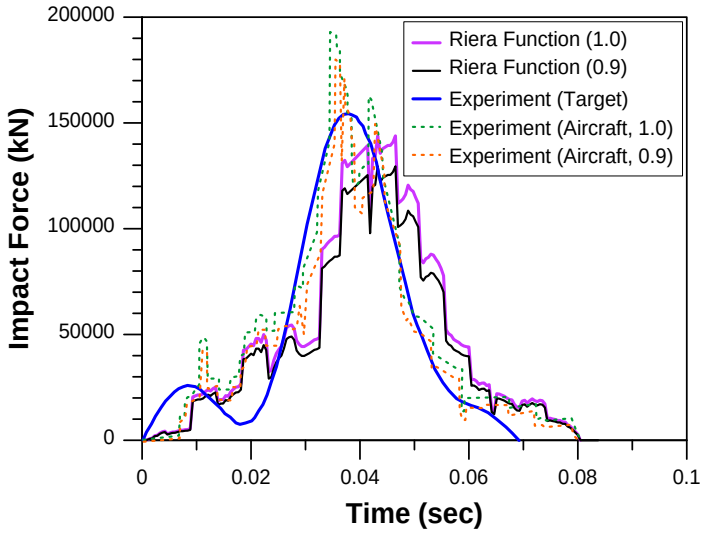

Figure 4-5 Impact Force from Riera Function

In **Figure 4-5**, the solid lines are the impact force of an aircraft in ANSYS LS-DYNA derived from the modified Riera function, while the dashed lines imply the results of the experiment. The aircraft impact force derived from the experiment was calculated from the Riera function including crushing force from **Eq. (2-13)**, while the target force was directly derived from the recorded data from the test. On the other hand, the impact force for the aircraft in this study showed similar tendency along with the mass distribution. The total duration of impact calculated by the Riera function was close to both the experiment and the results in this study because the Riera function is an approximate solution. The differences in magnitude was due to the crushing force.

At near 0.02 seconds, the impact force of the concrete target was slightly decreased and then rapidly increased up to the peak value at 0.04 seconds when the heaviest part of the aircraft reached the target. Considering that the heaviest part of the aircraft was approximately 9 m from the front of the aircraft, this part reached the target at 0.042 seconds by dividing 215 m/s of the initial velocity.

There are two reasons why the impact force was diminished at 0.02 seconds. First of all, the impact force significantly depended on the mass distribution of the F-4D jet. According to **Figure 4-4**, rocket and sleds were added at 3 m from the front of the aircraft. It means that this minor mass of the projectile can affect the records of the test; therefore, it is important to match the mass distribution of the numerical model with the mass used in the test.

The second reason is that the impact force was affected by the reaction behavior of the concrete at the same time when the target was impacted. According to Kang et al. (2016), the concrete target gives off compressive wave against the impact force which reaches to the rear surface of the target. In this way, the rear region shows compressive behavior followed by steady region when the compressive wave is almost equal to the tensile wave. In this experiment and numerical simulation, the scabbing failure of the concrete target was not recorded. Therefore, the decrease of the impact force at 0.02 seconds was due to the compressive wave by the inside of the concrete opposite to the impact direction. Then, this wave was immediately cancelled off because the huge mass of the aircraft was crushing into the target. Moreover, the scabbing failure was difficult to occur since the thickness of the target was 3.66 m.

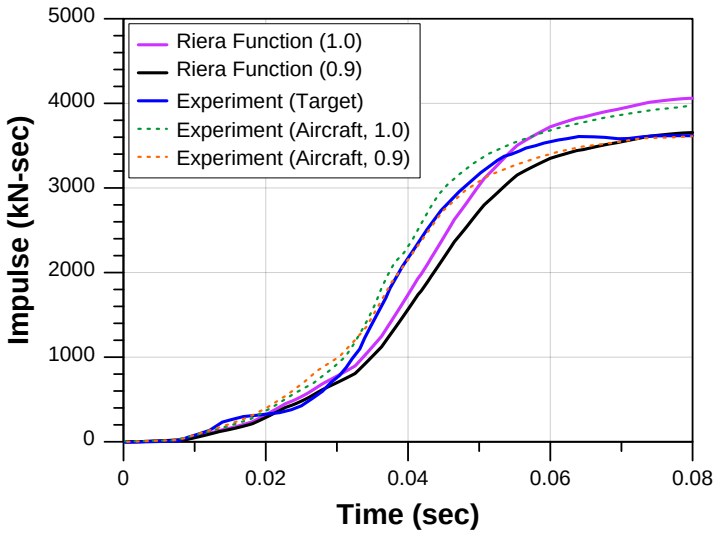

Figure 4-6 Impulse from Riera Function

The impulse results are demonstrated in **Figure 4-6**, which were calculated by integrating the impact force over time. Parts of the delayed impact force are reflected in the impulse near 0.04 second as shown in **Figure 4-5** to **Figure 4-6**. The impulse using the Riera function illustrates a similar pattern to that of the impulse in this study. This means that the mass distribution established by ANSYS LS-DYNA was significantly analogous to that of the F-4D model used in the experiment. As Sugano et al. (1993c) concluded, the effective mass coefficient of 0.9 was considerably matched with the performance of the target. The modified formula with $\alpha =$ 0.9 is close to the results of the experiment. It is concluded that Riera formula is accurate to evaluate the impact force for the projectile, and it is verified that 90% of the mass (α = 0.9) would be reflected during the impact. However, key results from the experiment are not response of the aircraft, but that of the target because the impact force of the aircraft evaluated by the Riera function contains distributed mass during the impact. This is why the effective mass coefficient (α) was introduced. It is necessary to compare results from analysis with responses of the target from the experiment as well as the results for mass distribution with the effective mass coefficient of 0.9.

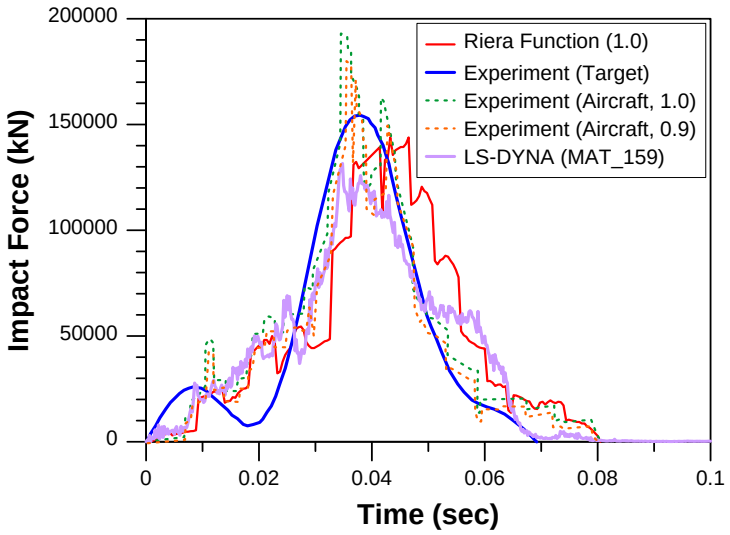

Figure 4-7 Impact Force from Numerical Analysis

Figure 4-7 depicts impact force of the numerical analysis compared to the experimental results and impact force derived from the Riera formula. The main object of the analysis was to compare the analytical results to the experimental results of the target since the target's behavior was mainly concerned. As shown in Figure 4-6, the tendency of the numerical results was similar to the experimental results.

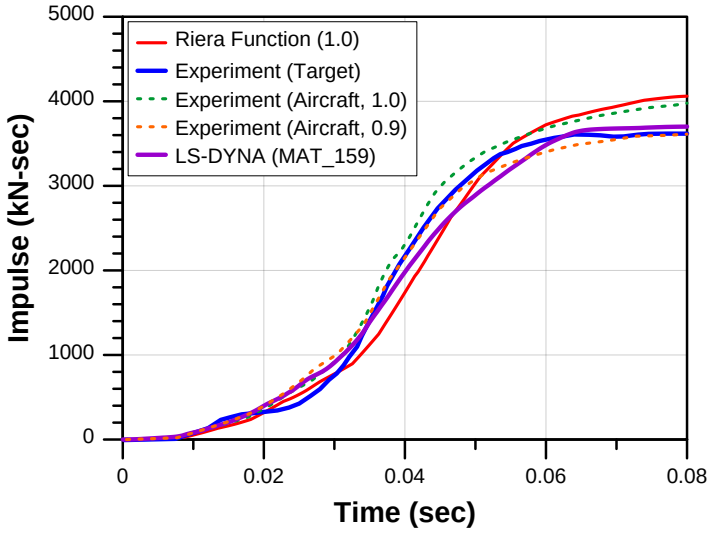

Figure 4-8 Impulse from Numerical Analysis

Figure 4-8 describes the impulse which was obtained by integrating the impact force along with time. The impulse from the numerical analysis shows considerably analogous to the experimental results. Furthermore, the numerical result is almost the same as the impulse of the aircraft with the effective mass coefficient (α) of 0.9.

In conclusion, from **Figure 4-7** and **Figure 4-8**, it is concluded that the impact force and impulse derived from analysis results of ANSYS LS-DYNA is analogous to the Riera function. The Riera evaluation shows exactly the same pattern of mass distribution of the SPH model. It is because the assumption of the Riera method is a projectile crushes into a rigid target and remains perpendicular to incidence. On the other hand, for reality and during the analysis, crushing parts can be affected by surrounding situations. It shows similar graphs between the analysis result and the Riera function. At 0.06 seconds, the impact force was dramatically decreased. It is regarded due to reflected and penetrated particles during the simulation. The numerical analysis in this study estimated the impact force correctly, and the result was reliable compared with the Riera approach.

As a further analysis, the tendency of the impact force and the impulse was figured out according to the various value of the FS parameter. According to the Lee et al. (2014), the FS of 1.8 displayed accurate results compared to others. However, the defined model between Lee et al. (2014) and this study were different in terms of the specified properties or the conditions of the numerical aircraft model.

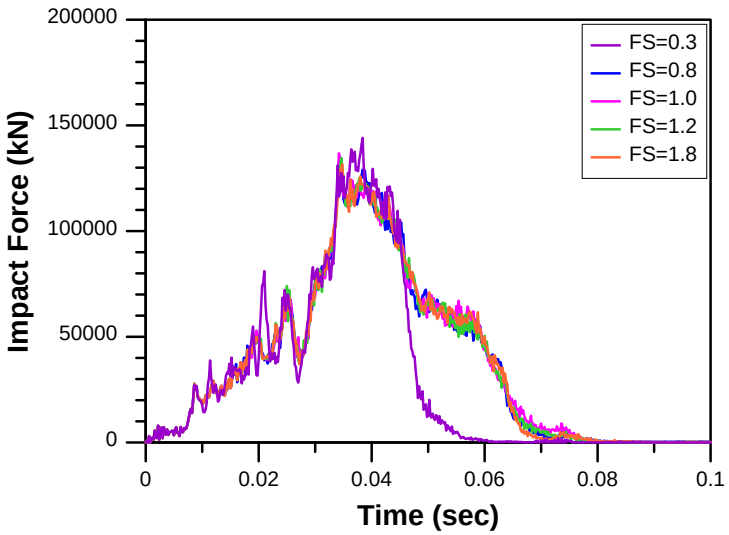

Figure 4-9 Impact Force with Various Failure Strains

The failure strain (FS) parameter implemented in the material keywords means the effective plastic strain when the elements start to be eroded (LSTC, 2016a). The selected values of the FS were 0.8, 1.0, 1.2, and 1.8.

As shown in **Figure 4-9**, the results of the impact force along with the various failure strain parameters were close to each other. It was assumed that the failure strain was not influential in the analysis to match with the test results. Even though Lee et al. (2014) discussed the most appropriate value of the FS, the determined conditions in the software would be different in various ways. Therefore, with the numerical conditions in this thesis, the failure strain was not concerned as a major parameter in the analysis.

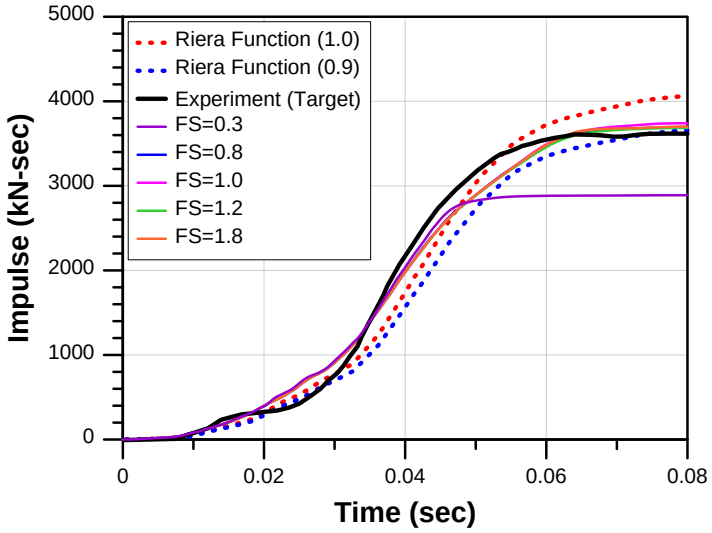

Figure 4-10 Impulse with Various Failure Strains

Figure 4-10 illustrates comparisons for the impulse in terms of the diverse value of the failure strain (FS). The result derived from the Riera function with the effective coefficient of 0.9 showed good agreement with the test result. Numerical results were almost the same regardless of the FS, and were located between the two results determined by the Riera function with different effective mass coefficient. It means that the numerical results showed variations within 10 % from the experimental results. Therefore, any failure strain parameters used in this further study can be adopted since the results with the variation of 10 % were roughly regarded as reliable conclusions.

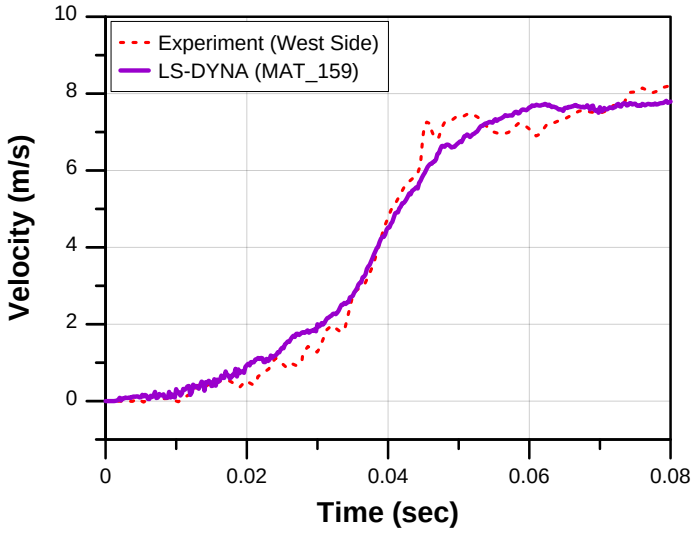

Figure 4-11 Velocity Comparison with Test

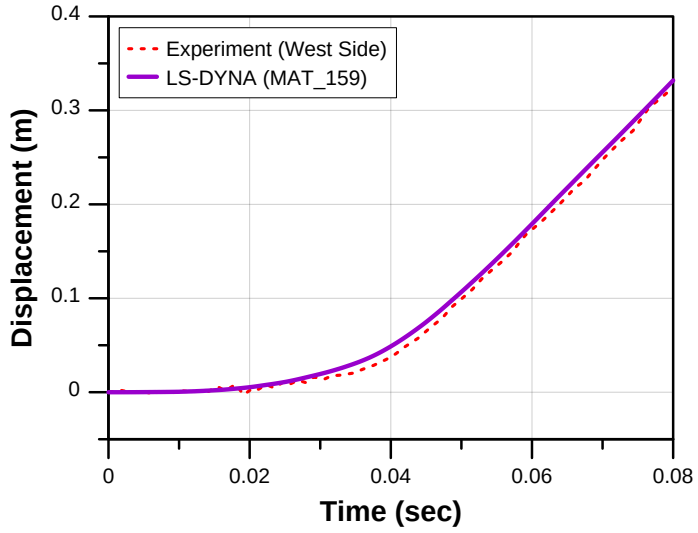

Figure 4-12 Displacement Comparison with Test

The velocity and displacement of the concrete target are demonstrated in **Figure 4-11** and **Figure 4-12**. It shows considerably similar patterns for both categories between the experiment and the analysis. Around 0.04 seconds, when the maximum impact force was recorded, both velocity and displacement rapidly increased. In summary, the numerical analysis using

ANSYS LS-DYNA can illustrate impact accidents with accurate results. In this regard, numerical analysis using ANSYS LS-DYNA is reliable.

Overall, the CSCM concrete model in ANSYS LS-DYNA showed good agreement with the performance of the target. The aircraft behavior was agreed well with the effective mass coefficient of 0.9. The numerical model using the SPH method is similar to the actual aircraft behavior. The failure strain (FS) of 1.8 turns out to be appropriate to be employed in numerical simulations.

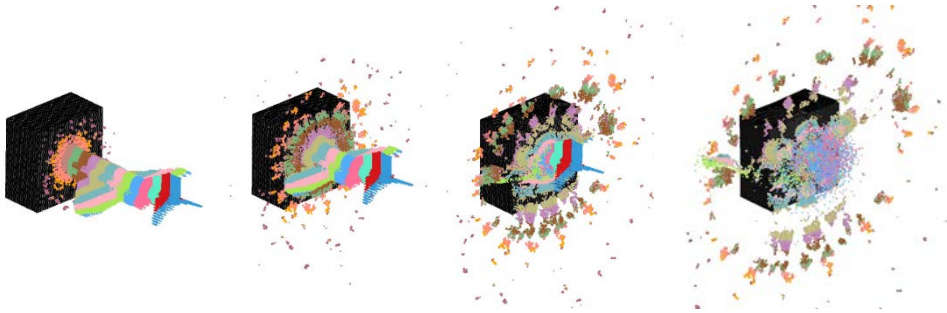

Figure 4-13 F-4D Impact Process during Impact

Figure 4-13 demonstrates effects of the aircraft impact on the concrete target at each step during the impact. The particles of the aircraft were mostly spread out at a crushing moment. At 0.08 seconds, some particles were not spread out significantly, likely due to the reaction of the reflected particles. It is speculated that it causes a significant drop in the impact force graph as seen in **Figure 4-7**.

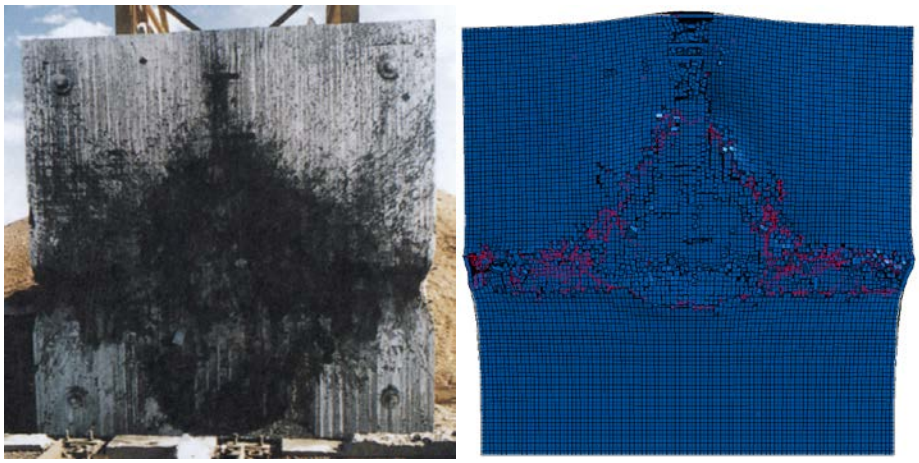

Figure 4-14 Concrete Target Failure Comparison

At the end of the simulation, concrete elements were deleted as shown in **Figure 4-14**. With comparison to the test target (1993), the penetrated shape is similar to the results of the test. The bottom of the impacted area was slightly different due to discrepancies in conditions between the analysis and the test. According to the Riera method, the total impacted area was regarded as twice the impact area of the projectile. For the experiment, the crushed area of fuselage of the F-4D aircraft was approximately 4.6 m^2, while the impacted area of the target was 10 m^2. In this study, the simulated impacted area of the target was approximately 10.14 m^2 which is quite close to of the experiment. These results give more confidence regarding the accuracy of the ANSYS LS-DYNA analysis and indicate that the prediction of the Riera method.

4.4 Discussion

This chapter aims to verify the F-4D Phantom crash experiment performed by Sandia National Laboratories (SNL) using LS-DYNA, a finite element software specialized in simulation with large deformation. In addition, the validity of Missile-Target Interaction Analysis (MTIA) method is confirmed by comparison with the Riera formula and the results of the experiment. In ANSYS LS-DYNA, there are several types of concrete models with different characteristics. In this study, MAT_159 was selected as a concrete material. Finally, the primary conclusions drawn from this research are listed below:

1) The Riera function is a typical approximate solution to evaluate impact force. It is based on the mass distribution of the projectile. In this study, the developed SPH aircraft model was consisted of several parts with unit length. Based on this mass distribution, the impact force derived from Riera formula showed good agreement with the results of the test. In addition to the Riera function, to get more accurate solutions the effective mass distribution factor (α) was introduced. From previous research, it was concluded that 0.9 is the suitable coefficient value for effective mass distribution. As a result, its reliability has been confirmed from this study.

2) At 0.02 seconds, the impact force for the experiment showed slightly diminished tendency. The speculated reasons were the mass distribution of the jet used in the test and the reaction response of the concrete target. From the results, it was speculated that the determined mass distribution of the projectile could influence the results. In addition, according to the previous study performed by Kang et al. (2016), the concrete generally shows compressive reaction opposite to the impact force. After that, the steady state was monitored as a result of the tensile wave due to the impact force. Considering that the target had the thickness of 3.66 m, the scabbing

failure was not easy to be happened.

3) With respect to the material properties of the aircraft, variable failure strain (FS) values can be determined in various ways. For this analysis, the FS of 1.8 was adopted because it was demonstrated to provide more reliable results than the others. Lastly, the aforementioned conditions helped to evaluate impact force so that ANSYS LS-DYNA analysis produced relatively accurate results. In addition to the aircraft impact accidents, it can be extensively expanded into other types of impact simulations.

Chapter 5. Numerical Analysis of Projectile Impact on Nuclear Structures

5.1 Introduction

Recently, the operation of Kori unit number 1 was totally stopped in June 2017 because of the end of its expected operating life. The Kori power plant is one of the oldest Nuclear Power Plants (NPPs) in Korea. It is reported that 51% of all Nuclear Power Plants (NPPs) in the world are over 30 years in operation. Deterioration of the NPPs is now the main stream around the world. In the future, permanent operation stop will increase.

As one of application plans for the closed NPPs, a complex combined with other renewable energy plants can be an alternative. In fact, the complex of the seashore wind turbine and the nuclear containment nearby the ocean has increased rapidly. Instead of the deconstruction, several wind turbines can be constructed on the ocean nearby the Kori plant and be operated by using electricity from the shut-downed plant. The previous examples about the complex with NPPs include Genkai nuclear plant in Japan and Maanshan plant in Taiwan. Reportedly, the wind plants were constructed within 1 kilometer from these nuclear plants. From these examples, it appears that wind plants do not cause safety peril issues.

In the planned Kori complex with wind plants in Korea, the distance between wind turbines and the NPP is almost 1.8 kilometers. Even though the probabilities of the fractured blade impact are extremely small, consideration of blade accidents caused by the fragment of blades is important to secure the safety of the existing nuclear structure. A specific situation is assumed such that one of these fragments would reach the exterior wall of the nuclear

auxiliary building.

In the case of overseas wind turbine failure accidents, the power plant of 660 kW in Burgos, Spain was destroyed in 2000 due to the blade impact. The fragment of the blade moved almost 1000 m distance. In 2003, one of the plants in Germany was collapsed by heavy rain and the fragment of the blade was found in 500 m distance. The most notable fact was that a house was located within 400 m in the opposite direction. It means that there was possibility of the damage of human life. In 2008, Danish wind power plant's blade was broken by strong wind. Many accidents were also reported in Korea. For instance, accidents occurred in Jeju in 2010 and 2015, and in Gangwon-do Province in 2016. It indicates that the blade accidents are no longer special issues which has been only reported in overseas.

The main concern of this numerical study is to perform numerical analysis on an auxiliary building under projectile impact. The overall responses of the reinforced concrete structure are observed based on the results of the analysis. Another analysis is to impact on single walls with various wall thicknesses in order to predict the behavior of the structure depending on the thickness. Structural safety can be verified and determined according to these analyses. The results of the analysis are then verified using existing equations to evaluate local failure. The energy-based penetration model recently developed by Hwang et al. (2017) is used to predict penetration occurrence and to verify reliability of the analytical results.

5.2 Accident Scenario

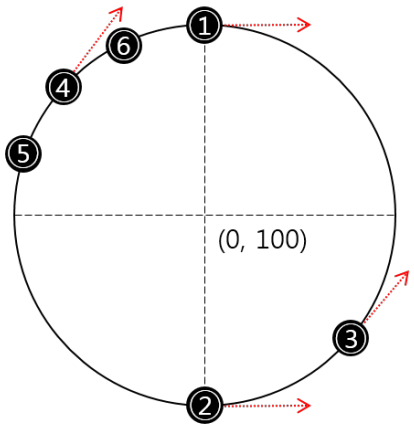

Figure 5-1 Diverse Scenarios for Blade Fracture Accidents

Preliminary simulations were performed according to supposed 6 cases to examine the scattering distance of the blade piece as described in **Figure 5-1**. The cases are based on where the failure of the blade will occur during rotation. To perform substantially reliable analysis, the preliminary simulations involve additional conditions such as missile drag coefficient (C_D), air density (ρ_{air}), water surface exposure coefficient (α_w), 3-second peak gust wind speed (V_h^{open}), and initial velocity of missile. The simulations were conducted by Korea Electric Power Corporation Engineering & Construction (KEPCO-ENC) company in advance.

As a result, the fourth case was regarded as a perilous scenario among a wide variety of accident cases. The maximum distance from the spot where the projectile reaches was less than 1 km. In this regard, it is speculated that the blade projectile would not reach the nuclear power plant directly. Even though the blade impact is improbable, the numerical analysis was conducted assuming the impact accident might occur since some instances including over 1 km distance have been reported from abroad.

5.3 Numerical Model in LS-DYNA

5.3.1 Numerical Modeling

The unit consistency of the received auxiliary structure is slug for mass, feet for length, second for time, and pound per square feet for stress. However, the CSCM model provides users with only five available unit options. To match with unit options embedded in the concrete model, the concrete auxiliary building is scaled down from feet to meter in terms of the length. Finally, the converted unit consistency was kilogram for mass, meter for length, second for time, newton for power, and Pascal for stress. The dimensions of the auxiliary building were 68.58 m in wide, 41.15 m in depth, and 49.07 m in height. **Figure 5-2** illustrates numerical modeling established in ANSYS LS-DYNA.

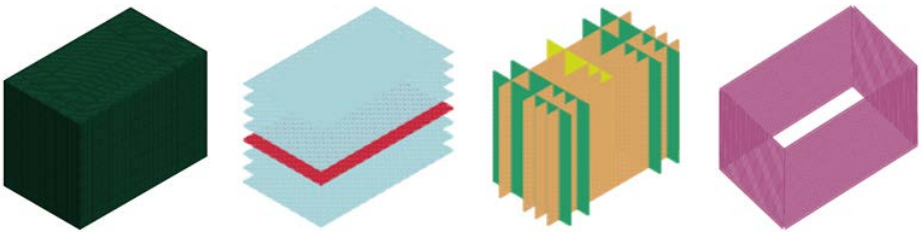

(a) Concrete Containment | (b) Horizontal Reinforcement | (c) Vertical Reinforcements | (d) External Reinforcements

Figure 5-2 Numerical Modeling of Auxiliary Structure in ANSYS LS-DYNA

The material keyword for the auxiliary structure was defined using CSCM model since this concrete model is for numerical analyses of the impact or blast accidents. Its analytical reliability was already verified by other researchers (Seo and Noh, 2013). Furthermore Chung et al. (2010) concluded that CSCM model showed good analytical results compared to the experimental results.

The remarkable characteristic of CSCM model is the erosion effect. In general, the value of ERODE card implemented in CSCM keyword is between 1.05

and 1.1. The specific value over unity means that the concrete elements would be deleted when strain of the concrete reaches maximum principal strain. The compressive strength of the concrete was determined by reverse calculating from the provided modulus of elasticity of the concrete. According to ACI 318-14 (2014), the modulus of elasticity of the concrete (E_c) for normal weight was estimated as below:

$$E_c = 4700\sqrt{f_c'} \quad \text{(MPa)} \tag{5-1}$$

where f_c' is the compressive strength of the concrete. From **Eq. (5-1)**, 50.8 MPa was given to the compressive strength of the concrete auxiliary building.

Table 5-1 Material Properties for Auxiliary Building

	Density (kg/m^3)	Modulus of Elasticity (GPa)	Compressive Strength (MPa)	Yield Stress (MPa)	Poisson's Ratio
Concrete	2400	33.75	50.8	-	-
Steel	7850	200	-	-	0.3

The area of 10.06 cm^2, 14.51 cm^2, and 43.55 cm^2 was employed for each reinforcements. The material keyword of the rebar was defined as plastic kinematic model (MAT_003). The beam elements were constructed as truss elements considering conservative aspects. CLIS keyword was employed to simulate the reinforcement embedded in the concrete structure.

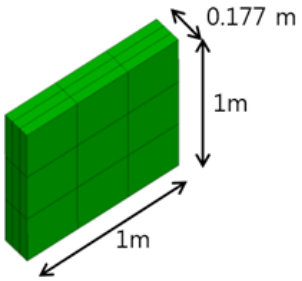

Figure 5-3 Blade Fragment Model

As shown in **Figure 5-3**, the projected area of the blade fragment was 1 m^2, and 300 kg for mass. The material properties of FRP are listed on **Table 5-2**. The values at each parameter were determined based on the Lee et al. (2012), and Tavarez et al. (2003). Considering the density of the Fiber-reinforced Polymer (FRP) was 1700 kg/m^3, the length of the crashing blade fragment was determined as 0.177 m using the solid element.

Table 5-2 Material Properties for Blade Projectile

	Density (kg/m^3)	Modulus of Elasticity (GPa)	Poisson's Ratio
Blade (MAT_001)	1700	24.6	0.3

In this study, the material of the blade was assumed as a Fiber-Reinforced Polymer (FRP). The LS-DYNA contains typical material keywords for FRP material including MAT_054 (Enhanced Composite Damage model) and MAT_002 (Orthotropic Elastic model). However, in this thesis, the piece of the blade was made of MAT_001 (Elastic model) keyword to consider conservative aspects. In this material model, the failure of the specified material does not occur until the supplementary keyword, which is MAT_ADD_EROSION to create failure effect, is accepted for the specified elastic model.

As concluded in **Section 5.2**, the most critical accident case was the fourth case in terms of the maximum distance of the projectile. Moreover, the maximum speed of the projectile was monitored in the fourth case. The conditions for the numerical analysis was based on the results of the fourth case. The impact velocity of the constructed projectile was set to 100 m/s which was similar to the maximum speed of the fourth case. The normal direction to the wall was assumed to perform the numerical simulation under conservative conditions even though the vertical impact to the wall is improbable in the actual accidents. It was because the structural safety evaluation should be conducted considering the most severe accidents.

The velocity of the projectile in LS-DYNA was defined by using INITIAL_VELOCITY keyword. The contact algorithm between the blade projectile and the impact surface of the auxiliary structure was determined using AUTOMATIC_SURFACE_TO_SURFACE keyword. The area of the blade projectile was defined as a slave part, while the front surface of the auxiliary structure was for a master part.

5.4 Analysis Results

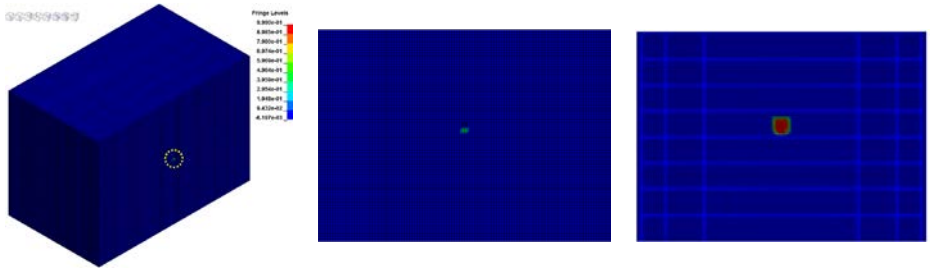

(a) Overall Structure (b) Front Surface (c) Rear Surface

Figure 5-4 Numerical Modeling of Auxiliary Structure in ANSYS LS-DYNA

Figure 5-4 displays the overall responses of the auxiliary structure due to the blade impact simulation. Compared to the huge size of the structure, the blade projectile did not create critical influence. Large strains of the concrete were monitored at the rear surface rather than the front surface. It is speculated that since the projectile shape was rectangular, insignificant strains were obtained at the front side. Furthermore, since the element was not deleted in the software, there was no scabbing failure, no perforation failure, and no residual speed of the projectile during the simulation. In conclusion, the structural integrity of the auxiliary building is not affected considerably by the blade projectile impact.

At the front surface, the strain of the concrete was steady after 0.004 seconds. The initial strain change was monitored at 0.002 seconds when the blade projectile collided onto the surface simultaneously. On the other hand, the strain of the rear side was increased since 0.003 seconds. The area where the strain change was monitored was significant for the rear surface.

5.5 Local Failure

Not only overall response of the auxiliary building subjected to blade projectile but also the local failure of the wall as part of the building need to be confirmed meticulously. Another reason of the additional analysis for the representative wall thicknesses was to reduce computational cost monitored during the analysis to recognize overall behavior of the auxiliary structure.

5.5.1 Numerical Modeling

The mostly concerned variable was the thickness of the wall. Four thicknesses were selected from 2 feet to 5 feet (0.61 m to 1.52 m). The concrete wall was sized down with 1:2 scale in order to gain visualized effects about concrete cross section along the thickness direction. Considering the actual layout of the concrete wall, identical covering depth and the sectional area of the steel were considered. The size of the wall was 20 feet by 10 feet (6.1 m by 3.05 m) with respect to 1:2 scale as shown in **Figure 5-5**.

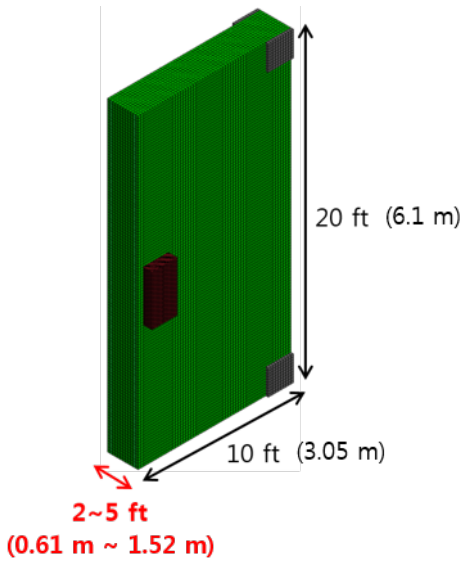

Figure 5-5 Numerical Modeling of Auxiliary Structure in ANSYS LS-DYNA

The concrete target was constructed using the CSCM (MAT_159) which is one of the most popular concrete models in the ANSYS LS-DYNA. Meanwhile, the kinematic elastic model (MAT_003) was employed for reinforcement bars. The FRP was assumed for the blade projectile. Pertinent elastic and inelastic material models for FRP are available in the ANSYS LS-DYNA such as the orthotropic elastic model (MAT_002), the composite damage model (MAT_022), and the enhanced composite damage model (MAT_054). In this thesis, however, the elastic model (MAT_001) without failure was utilized for the blade fragment considering conservative analysis conditions.

The boundary conditions were important since the constructed model was the half parts of the entire concrete wall. The boundary conditions for the plane of symmetry should be exactly specified considering behavior of the other side. One out-of-plane displacement (*yz* plane) and two out-of-plane moment for the *y*-axis and *z*-axis were constrained considering the symmetry.

Four supports were established using RIGID material to constrain support positions without deformation or erosion. The contact algorithm between each support and the surface of the concrete panel was determined using AUTOMATIC_SURFACE_TO_SURFACE keyword. The slave part was the concrete panel and the master part was supports. Contact algorithm between the blade projectile and the typical concrete panel was specified identically as the numerical analysis for the whole auxiliary structure.

5.5.2 Analysis Results

Figure 5-6 indicates the results of the numerical analysis for the typical wall thicknesses. The opposite part of the wall which was not constructed in LS-DYNA considering 1:2 scale was clearly demonstrated using mirror effects implemented in LS-DYNA. In other word, the changes of the left size is identical to the right size which was modeled in advance.

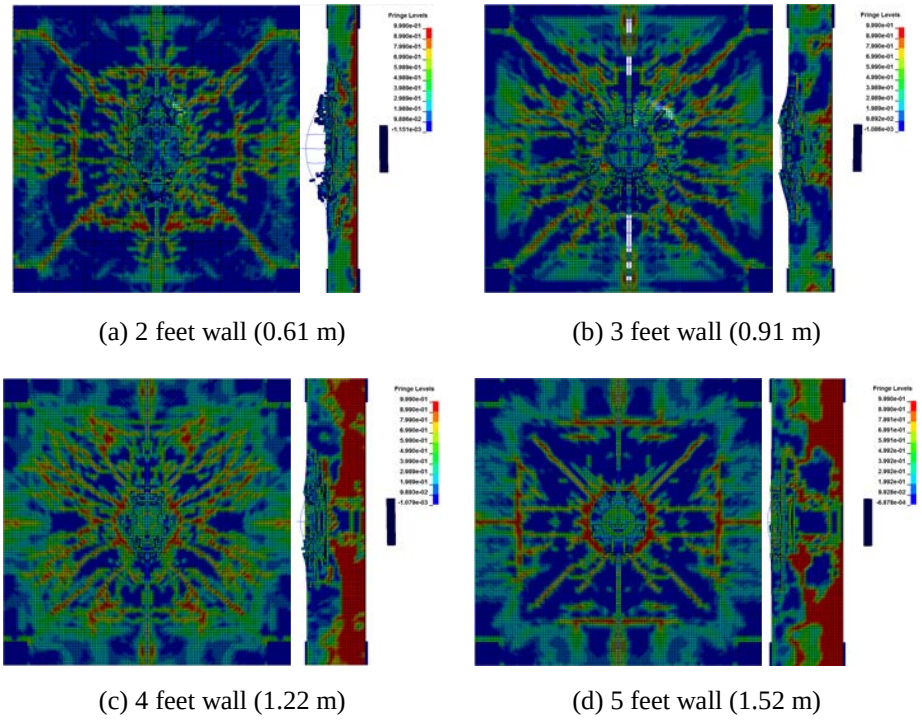

(a) 2 feet wall (0.61 m) (b) 3 feet wall (0.91 m)

(c) 4 feet wall (1.22 m) (d) 5 feet wall (1.52 m)

Figure 5-6 Analytical Results for Single Wall (0.61 m to 1.52 m)

As shown in **Figure 5-6**, the number of the deleted elements was reduced as the thickness of the wall increased. For all thicknesses, the perforation and the residual velocity were not monitored, but the scabbing failure was founded in the results. The area of the scabbing failure at rear face of the concrete targets was diminished as the thickness of the target increased. Contrary to the overall responses, each wall showed the scabbing failure, but this failure became gradually smaller as the thickness increased.

Table 5-3 Effective Plastic Strain of Concrete Wall

Wall Thickness	0.01 sec	0.02 sec	0.03 sec	0.04 sec
2 feet (0.61 m)	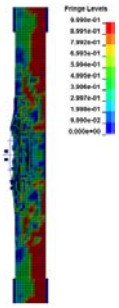	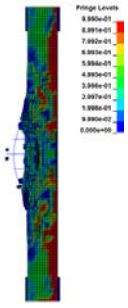	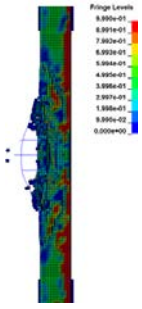	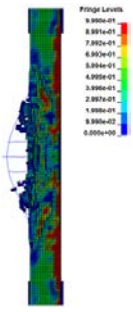
3 feet (0.91 m)	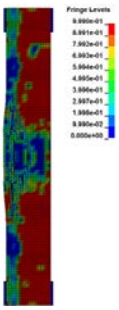	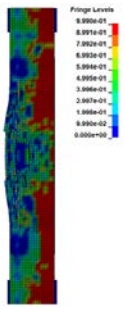	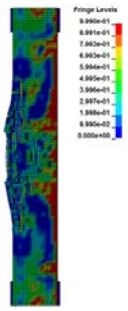	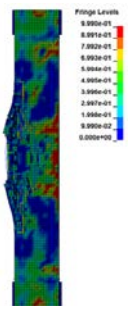
4 feet (1.22 m)	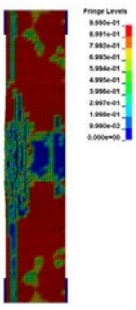	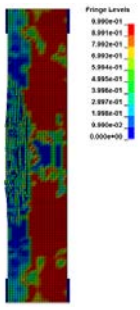	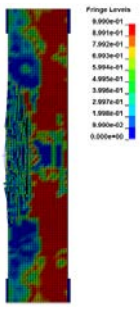	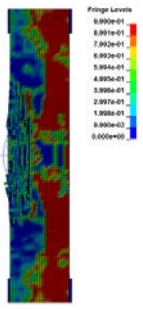
5 feet (1.52 m)	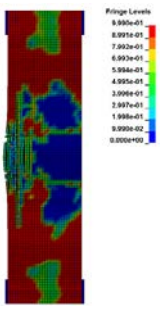	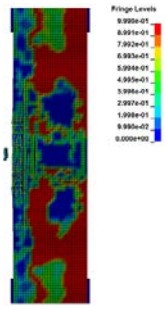	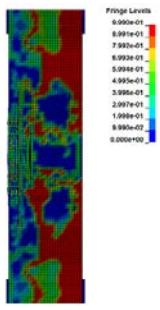	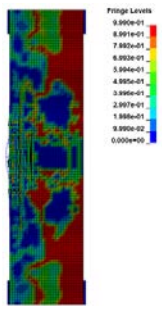

Table 5-3 indicates the effective plastic strain of the concrete targets during the impact. The crashed surface when the projectile impact occurs in reality is the external surface of the structure. The actual auxiliary structure has 5 feet (1.52 m) of the wall thickness for the external wall. According to the analytical results, there were no perforation and residual velocity for 5 feet (1.52 m) of the thickness. Furthermore, the wall of the actual structure is significantly constrained by surrounding members including rebar, slab, or wall. In this analysis, each wall did not involve restraining factors as the structural conditions. Therefore, it is concluded that not only the probability of the severe accident is extremely rare but also the critical failure of the auxiliary structure will not be happened considering the severe scenario.

5.5.3 Limit Thickness for Scabbing and Perforation

To verify the reliability of the analytical results, comparison to the evaluation using diverse empirical equations was carried out. For scabbing limit thickness (h_s), ACE, Bechtel, BRL Chang, CRIEPI, Hughes, Modified NDRC, Modified Petry equation were selected. For perforation limit thickness (h_p), Degen equation substituted Bechtel equation since the Bechtel equation involves only the scabbing limit thickness (h_s), while the Degen equation defines only the perforation limit thickness (h_p). The required variations for each empirical equation was same as the numerical analysis such as initial velocity, mass, the compressive strength of the concrete, and modulus of elasticity of the projectile.

Table 5-4 Calculated Scabbing Limit Thickness

	h_s	2 feet (0.61 m)	3 feet (0.91 m)	4 feet (1.22 m)	5 feet (1.52 m)
	$h_{s,calc}$ (m)	Ratio ($h_s/h_{s,calc}$)	Ratio ($h_s/h_{s,calc}$)	Ratio ($h_s/h_{s,calc}$)	Ratio ($h_s/h_{s,calc}$)
ACE	2.820	0.216	0.322	0.432	0.539
Bechtel	0.535	1.139	1.699	2.278	2.838
BRL	0.051	11.919	17.781	23.839	29.701
Chang	0.556	1.096	1.635	2.192	2.731
CRIEPI	0.529	1.152	1.719	2.305	2.872
Hughes	0.461	1.322	1.972	2.644	3.294
Modified NDRC	0.978	0.623	0.930	1.247	1.553
Modified Petry	0.039	15.466	23.072	30.932	38.538

Table 5-4 articulates calculated scabbing limit thickness ($h_{c,calc}$) determined from the diverse empirical equations listed in the table considering the thickness of the panels. In general, the scabbing limit thickness (h_s) indicates the minimum thickness when the scabbing failure would not occur. For all thicknesses, the numerical analysis through LS-DYNA showed the scabbing failure. It means that when the thickness of the wall is from 2 feet to 5 feet (0.61 m to 1.52 m), the scabbing limit thickness should be above the wall thickness.

In **Table 5-4**, the scabbing limit thickness (h_s) is the wall thickness as a standard criteria. If the ratio of the scabbing limit thickness to the calculated scabbing limit thickness ($h_s/h_{s,calc}$) is close to the unity, the prediction of the used empirical equation is relatively accurate. If the ratio ($h_s/h_{s,calc}$) shows below the unity, the adopted empirical equation predicts the expected scabbing limit thickness conservatively. It is because the calculated scabbing limit thickness ($h_{s,calc}$) from the empirical equations is above the wall thickness (h_s), which showed the scabbing failure in all thicknesses (0.61 m to 1.52 m). On the other hand, if the ratio ($h_s/h_{s,calc}$) is over the unity, it means that the scabbing failure would not occur at the each wall thickness according to the empirical equation.

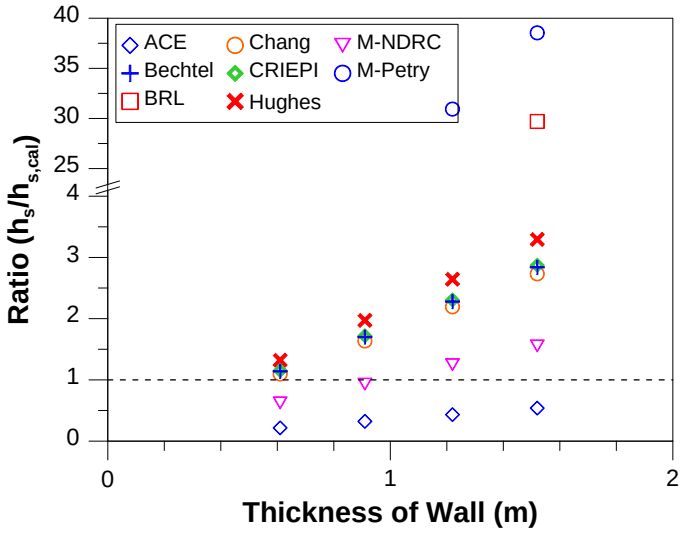

Figure 5-7 Ratio of Scabbing Limit Thickness ($h_s/h_{s,calc}$)

The summarized results in **Table 5-4** are depicted as a graph as shown in **Figure 5-7**. Below the unity indicates the scabbing failure would occur at each wall thicknesses, while above the unity means the scabbing failure would not occur according to the empirical equations which indicates against the results of the numerical analysis. According to the results evaluated from the modified NDRC equation, which is addressed in NEI 07-13 (2011), the equation predicts that the scabbing failure occurs for the thickness of 2 feet and 3 feet (0.61 m and 0.91 m). However, for the thickness of 4 feet and 5 feet (1.22 m and 1.52 m), the prediction shows no scabbing failure. Compared to other empirical equations, the modified NDRC equation is close to the unity. Therefore it is concluded that the modified NDRC formula is more reliable than others.

Table 5-5 Calculated Perforation Limit Thickness

	h_p	2 feet (0.61 m)	3 feet (0.91 m)	4 feet (1.22 m)	5 feet (1.52 m)
	$h_{p,calc}$ (m)	Ratio ($h_p/h_{p,calc}$)	Ratio ($h_p/h_{p,calc}$)	Ratio ($h_p/h_{p,calc}$)	Ratio ($h_p/h_{p,calc}$)
ACE	1.958	0.311	0.464	0.622	0.776
BRL	0.033	18.337	27.356	36.675	45.694
Chang	0.214	2.840	4.237	5.680	7.077
CRIEPI	0.193	3.155	4.708	6.311	7.864
Degen	0.671	0.908	1.354	1.816	2.263
Hughes	0.332	1.836	2.739	3.672	4.576
Modified NDRC	0.419	1.456	2.173	2.913	3.629
Modified Petry	0.035	17.012	25.379	34.025	42.392

Table 5-5 addresses the calculated perforation limit thickness ($h_{p,calc}$) from the previously proposed various equations. The actual wall thicknesses are assumed as the perforation limit thicknesses (h_p). The perforation limit thickness (h_p) means the least thickness when the perforation failure would not occur against the impact and is generally smaller than the scabbing limit thickness (h_s). The ratio between two criteria ($h_p/h_{p,calc}$) is determined by dividing wall thickness by the calculated perforation limit thickness.

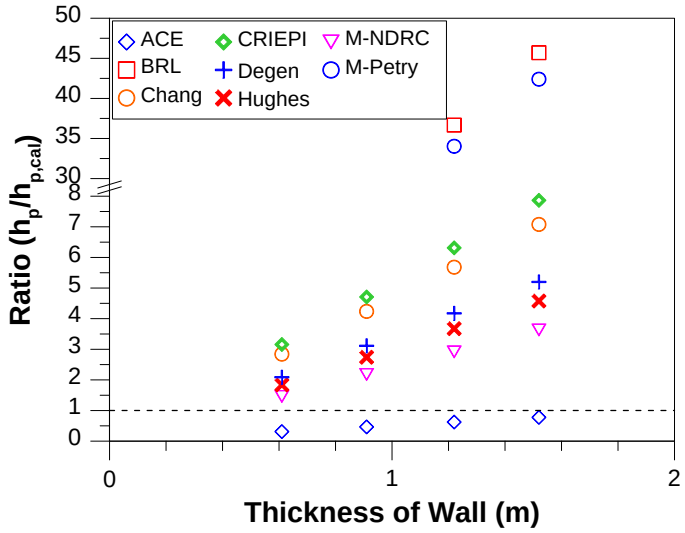

Figure 5-8 Ratio of Perforation Limit Thickness ($h_p/h_{p,calc}$)

Figure 5-8 depicts the ratio ($h_p/h_{p,calc}$) according to the previously proposed empirical equations. As shown in **Figure 5-6**, most of the previous equations predict that the perforation failure would not appear, including the most conservative modified NDRC equation mentioned in the NEI 07-13 (2009) expect the ACE equation. Only for the ACE equation, the prediction demonstrates that the perforation failure through the wall would happen. According to the modified NDRC equation, all the results are relatively close to the unity compared to other equations and consistent with the results of the numerical analysis. In this regard, the modified NDRC equation may be the most reliable empirical formula among aforementioned proposed equations.

5.5.4 Results of the Energy-Based Penetration Model

In this thesis, the energy-based penetration model suggested by Hwang et al. (2017) was utilized to determine the penetration depth (x) and the perforation failure of the concrete target. The required parameters were the size of concrete target, the material properties of concrete and reinforcement, the properties of the projectile, and the conditions for the impact. The four parameters were fixed in this study except for the size of the concrete. All the

concrete targets were 20 feet by 20 feet (6.1 m by 6.1 m) identically, but the thickness of the target was varied along from 2 feet to 5 feet (0.61 m to 1.52 m).

For the concrete, the compressive strength (f_c') was 50.8 MPa, the tensile strength (f_r) was 4 MPa, the density was 2400 kg/m^3, and the maximum aggregate size was 25 mm. The reinforcement embedded in the target was assumed to have the minimum longitudinal ratio of 0.004, considering the conservative aspects, and the yield strength of 400 MPa. The Fiber-Reinforced Polymer (FRP) of the blade had 1750 kg/m^3 for the density, 205 GPa for the modulus of elasticity, and 300 kg of the weight. Lastly, it was supposed as the condition of the impact that the projectile crashed into the target perpendicularly regarding the conservative features.

Table 5-6 Prediction of Penetration Depth (x) and Perforation Failure

Thickness	h/d	Effective Rebar Area (mm^2)		E_K/E_R	x (mm)	Perforation
		Front	Rear			
2 feet (0.61 m)	0.61	5944	5944	0.734	472.9	None
3 feet (0.91 m)	0.915	15088	15088	0.226	139.1	None
4 feet (1.22 m)	1.22	26593	26593	0.108	112.4	None
5 feet (1.52 m)	1.525	40020	40020	0.066	101.3	None

The results derived from the energy-based penetration model are summarized in **Table 5-6**. As shown in the table, the perforation failure did not occur in all thicknesses. The penetration depth (x) observed from the model with the wall thickness of 2 feet (0.61 m) was larger than the models with other thicknesses. It is because the case of the 2 feet (0.61 m) thickness had a small h/d value.

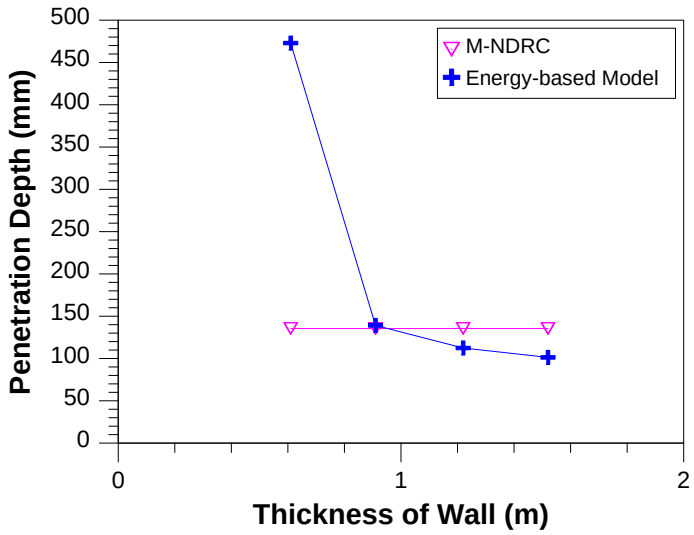

Figure 5-9 Penetration Depth (*x*) Comparison

Figure 5-9 depicts the comparison of the penetration depths (*x*) drawn from the energy-based penetration model proposed by Hwang et al. (2017) and the modified NDRC equation addressed in NEI 07-13 (2009). As shown in **Figure 5-9**, the specific result for the 2 feet (0.61 m) thickness presented a significant gap, but the similar predictions were monitored from 3 feet to 5 feet (0.91 m to 1.52 m) thickness. Particularly, the results calculated by the modified NDRC formula showed comparable results regardless of the wall thickness, while the results drawn from the energy-based penetration model tended to decrease as the thickness increased. It is speculated that the modified NDRC equation does not consider the ratio of *h*/*d*.

5.6 Discussion

In **Chapter 5**, the numerical analysis of the blade impact on the concrete auxiliary structure was performed using ANSYS LS-DYNA. The main purpose of the numerical analysis was to figure out structural behavior of the specified structure during the impact. The analysis consisted of two major parts. One was the structural evaluation for the overall auxiliary structure and the other was the local failure of the single wall based on the varied thicknesses which have actually been employed in the auxiliary structure. In summary, several conclusions are made as below:

1) First, the preliminary analysis was performed to determine the distance of the projectile considering adjacent environmental conditions. For the 6 cases, all of them showed the distance within 1 km. Therefore, the blade projectile would not reach to the auxiliary building even due to severe accidents in reality, given the specified separation.

2) During the impact, the concrete auxiliary building showed no scabbing failure, no perforation failure, and no residual velocity of the projectile under the conservative impact conditions. Moreover, the impact accident influenced the rear surface to greater extent than the front surface.

3) As a further study, the representative walls were selected. The various thicknesses were considered from 2 feet to 5 feet (0.61 m to 1.52 m). Under the identical analysis conditions, the perforation failure and residual velocity were not discovered from the specified four walls. Moreover, the analytical conditions contained many conservative factors including simplified boundary condition or the improbable initial velocity. In this regard, the serious accidents due to the blade projectile would be unlikely to happen in reality.

4) The numerical results were compared to the prediction using a wide variety of empirical equations and the recently developed energy-based penetration model. Among the empirical equations, the modified NDRC equations showed relatively accurate prediction that is consistent with the numerical results as well as the energy-based penetration model. In this regard, the modified NDRC equation and the energy-based model can be reliably utilized to predict the local failure of the concrete target for various cases.

Chapter 6. Conclusions

Concrete is one of the most popular materials for construction of a variety of structures. Among various concrete structures, Nuclear Power Plants (NPPs) are the essential structure that should be meticulously designed against severe impact. From the previous accidents including Three Mile Island in 1979 or Fukushima accident in 2011, it is learned that such severe accidents require a huge amount of time and cost to recover. The relevant design codes have been improved based on these accidents. For instance, the evaluation of the aircraft impact was adopted since the terror of the World Trade Center in 2001 in U.S.

The primarily concerned subject addressed in this thesis is to investigate the behavior of concrete structures under the aircraft impact and the projectile impact. According to the previous studies, the key factor for the local damage of the concrete subjected to aircraft impact was not the fuselage, but the engine. To broadly investigate the local impact damage, two different numerical analyses were carried out in this thesis: F-4D jet impact on concrete panel and blade impact on an auxiliary building which is a component of NPPs.

The primary conclusions and perspectives drawn from the present study are summarized as follows:

1) The results of F-4D jet impact using SPH approach showed relatively good agreement with the test results. Also, the value of 0.9 for the effective mass distribution factor (a) and 1.8 for failure strain (FS) of the aircraft material are turned out to be appropriate in order to obtain more reliable results.

2) For the local failure analysis, there were no structural failure and

residual velocity of the projectile, but some degree of scabbing failure of the wall. However, considering the overly conservative analytical conditions and boundary condition of actual structures, there would be no critical failure, expected in reality.

3) The modified NDRC equation predicted the scabbing failure in 2 feet and 3 feet (0.61 m and 0.91 m) wall, but no scabbing failure in 4 feet and 5 feet (1.22 m and 1.52 m) wall. Furthermore, it predicted no perforation failure for all thicknesses. According to the recently developed energy-based penetration model, there would be no perforation failure for all thicknesses. This is consistent with the results from the numerical analysis. The energy-based penetration model could be widely used to predict the occurrence of perforation of concrete targets and the residual velocity of projectiles.

4) The results derived from the numerical analysis appeared to be reliable enough and showed similar tendency compared to the previous empirical equations and the proposed energy-based penetration model. In this regard, the numerical conditions discussed in this thesis are appropriate and are expected to produce good prediction for similar local damage of various concrete structures.

References

1. ACI Committee 214 (2011), Guide to Evaluation of Strength Test Results of Concrete (ACI 214R-11), American Concrete Institute, Farmington Hills, MI, U.S.A.

2. ACI Committee 318 (2014), Building Code Requirements for Structural Concrete (ACI 318-14) and Commentary (ACI 318R-14), America Concrete Institute, Farmington Hills, MI, U.S.A.

3. ACI-ASME Joint Committee (2015), ASME Boiler and Pressure Vessel Code Section III-Division 2 and ACI Standard 359, The American Society of Mechanical Engineers, New York, NY, U.S.A.

4. Amirikian A. (1950), Design of protective structures (Report NT-3726), Bureau of Yards and Docks, Department of the Navy, Washington, DC, U.S.A.

5. Arros, J. and Doumbalski, N. (2007), "Analysis of Aircraft Impact to Concrete Structures," *Nuclear Engineering and Design 237*, 1241-1249.

6. ASTM C39 (2005), Standard Test Method for Compressive Strength of Cylindrical Concrete Specimens, Annual Book of ASTM Standard, West Conshohocken, PA, U.S.A.

7. Bang, C.-J. (2014), "A Study on Nuclear Power and Nuclear Construction Technology Trend for Enhancement of Competitiveness in Nuclear Global Market", *Review of Architecture and Building Science*, V. 58, No. 7, pp. 8-11. (in Korean)

8. Belytschko, T., Ong, J. S. J., Liu, W. K., and Kennedy, J. M. (1984), "Hourglass Control in Linear and Nonlinear Problems," *Computer Methods in Applied Mechanics and Engineering*, V. 43, No. 3, 251-276.

9. Chang, W. S. (1981), "Impact of Solid Missiles on Concrete Barriers," *Journal of the Structural Division*, V. 107, No. 2, 257-271.

10. Chelapati, C. V., Kennedy, R. P., and Wall, I. B. (1972), "Probabilistic Assessment of Aircraft Hazard for Nuclear Structure," *Nuclear Engineering and Design*, V. 19, No. 2, 333-364.

11. Chung, C.-H, Choi, H., Lee, J. W., and Choi, K. R. (2010), "Evaluation of Local Effect Prediction Formulas for RC Slabs Subjected to Impact Loading," *Journal of the Korean Society of Civil Engineers*, V. 30, No. 6A,

543-560. (in Korean)

12. Degen, P. P. (1980), “Perforation of Reinforced Concrete Slabs by Rigid Missiles,” *Journal of the Structural Division*, V. 106, No. 7, 1623-1642.

13. Fang, Q. and Wu, H. (2017), Concrete Structures Under Projectile Impact, Springer Singapore.

14. fib Task Group 1.3 Containment Structures (2001), Nuclear Containments - State-of-the-Art Report, Bulletin 13, International Federation for Structural Concrete (fib), Federal Institute of Technology, Lausanne, Switzerland.

15. Hessheimer, M. F., Klamerus, E. W., Rightley, G. S., Lambert, L. D., and Dameron, R. A. (2003a), Overpressurization Test of a 1:4-Scale Prestressed Concrete Containment Vessel Model, NUREG/CR-6810, SAND2003-0840P, Sandia National Laboratories, Albuquerque, NM, U.S.A.

16. Hessheimer, M. F., Shibata, S., and Costello, J. F. (2003b), “Functional and Structural Failure Mode Overpressurization Tests of 1:4-Scale Prestressed Concrete Containment Vessel Model,” *Transactions of the 17th International Conference on Structural Mechanics in Reactor Technology (SMiRT 17)*, Prague, Czech Republic.

17. Hong, J.-K. and Kang, T. (2016), “A Study on Behavior of the Shell Structure under Inner Pressure,” *International Journal of Conceptions on Mechanical and Civil Engineering*, V. 4, No. 3, 35-38.

18. Hwang, H.-J., Kim, S., and Kang, T. H.-K (2017), “Energy-Based Penetration Model for Local Impact-Damaged Concrete Members,” *ACI Structural Journal*, V. 114, No. 5, 1189-1200.

19. IAEA (2003), Safety Standard Series: External Events Excluding Earthquakes in the Design of Nuclear Power Plants, Safety Guide No. NS-G-1.5.

20. Jiang, H. and Chorzepa, M. G. (2014), “Aircraft Impact Analysis of Nuclear Safety-Related Concrete Structures: A Review,” *Engineering Failure Analysis*, V. 46, 118-133.

21. Johansson, A. and Fredberg, J. (2015), "Structural Behaviour of Prestressed Concrete Beams During Impact Loading," Master’s Thesis, Department of Civil and Environmental Engineering, Chalmers University of Technology, Gothenburg, Sweden.

22. Kang, T. H.-K, Kim, S., Kim, M.-S., and Hong, S.-G. (2016), “Impact Resistance of UHPC Exterior Panels under High Velocity Impact Load,” *Journal of the Korea Concrete Institute*, V. 28, No. 4, 455-462. (in Korean)

23. Kar, A. K. (1979), “Impactive Effects of Tornado Missiles and Aircraft,” *Journal of the Structural Division*, V. 105, 2243-2260.

24. Kennedy, R. P. (1976), ″A Review of Procedures for the Analysis and Design of Concrete Structures to Resist Missiles Impact Effects,” *Nuclear Engineering and Design*, V. 37, 183-203.

25. Kim, S., Kang, T. H.-K, and Yun, H.-D. (2017), “Evaluation of Impact Resistance of Steel Fiber-Reinforced Concrete Panels Using Design Equations,” *ACI Structural Journal*, V. 114, No. 4, 911-921.

26. Klamerus, E. W., Bohm, M. P., Wesley, D. A., and Krishmaswamy, C. N. (2000), Containment Performance of Prototypical Reactor Containments Subjected to Severe Accident Conditions, NUREG/CR-6433, SAND96-2445, Sandia National Laboratories, Albuquerque, NM, U.S.A.

27. Kostov, M., Miloshev, M., Nicolov, A., and Klecherov, I. (2015), “Non-Structural Mass Modeling in Aircraft Impact Analysis Using Smooth Particle Hydrodynamics,” *10th European LS-DYNA Conference*.

28. Kojima, I. (1991), “An Experimental Study on Local Behavior of Reinforced Concrete Slabs to Missile Impact,” *Nuclear Engineering and Design*, V. 130, No. 2, 121-132.

29. Lee, K., Han, S. E., and Hong, J.-W. (2013a), “Analysis of Impact of Large Commercial Aircraft on a Prestressed Containment Building,” *Nuclear Engineering and Design*, V. *265*, 431-449.

30. Lee, K., Jung, J. W., and Hong, J. W. (2014), “Advanced Aircraft Analysis of an F-4 Phantom on a Reinforced Concrete Building,” *Nuclear Engineering and Design*, V. 273, 505-528.

31. Lee, K.-S., Kim, H.-J., and Han, S.-E. (2013b), “Aircraft Impact Theory and Mass Model for the Missile-Target Interaction Analysis of Large Aircraft,” *Journal of the Architectural Institute of Korea: Structure & Construction*, V. 29, No. 300, 27-34. (in Korean)

32. Lee, Y.-J., Jhan, Y.-T., and Chung C.-H. (2012), “Fluid–Structure Interaction of FRP Wind Turbine Blades under Aerodynamic Effect,” *Composites Part B: Engineering*, V. 43, No. 5, 2180-2191.

33. Li, Q. M., Reid, S. R., Wen, H. M., and Telford, A. R. (2005), “Local Impact Effects of Hard Missiles on Concrete Targets,” *International Journal of impact engineering*, V. 32, No. 1, 224-284.

34. Linderman R. B., Fakhari M., Rotz J. V. (1973), Design of Structures for Missile Impact (BC-TOP-9 Rev. 1), Bechtel Power Corporation, San Francisco, CA, U.S.A.

35. LSTC (2016a), LS-DYNA Keyword User’s Manual, Livermore Software Technology Corporation, Livermore, CA, U.S.A.

36. LSTC (2016b), LS-DYNA Theory Manual, Livermore Software Technology

Corporation, Livermore, CA, U.S.A.

37. Moon, I.-H. and Choi, C.-S. (2014), “Structural Characteristics and Design Specifications of Nuclear Power Plant Structures,” *Review of Architecture and Building Science*, V. 58, No. 7, 12-21. (in Korean)

38. Murray, Y. D., Abu-Odeh, A. Y., and Bligh, R. P. (2007), Evaluation of LS-DYNA Concrete Material Model 159 (No. FHWA-HRT-05-063), Federal Highway Administration, McLean, VA, U.S.A.

39. OECD/NEA/CSNI (2002), Specialist Meeting on External Hazards.

40. Remennikov, A. M. and Kong, S. Y. (2012), “Numerical Simulation and Validation of Impact Response of Axially-Restrained Steel–Concrete–Steel Sandwich Panels,” *Composite Structures*, V. 94, No. 12, 3546-3555.

41. Riera, J. D. (1968), “On The Stress Analysis of Structures Subjected To Aircraft Impact Forces,” *Nuclear Engineering and Design*, V. 8, No. 4, 415-426.

42. Schwer, L. (2011), “The Winfrith Concrete Model: Beauty or Beast? Insights into the Winfrith Concrete Model,” *8th European LS-DYNA Users Conference*, 23-24.

43. Schwer, L. E. and Malvar, L. J. (2005), “Simplified Concrete Modeling with *MAT_CONCRETE_DAMAGE_REL3,” *JRI LS-DYNA User Week*, 49-60.

44. Seo, D. W. and Noh, H. C. (2013), “Aircraft Impact Analysis of Steel Fiber Reinforced Containment Building,” *Journal of Computational Structural Engineering Institute of Korea*, V. 26, No. 2, 157-164. (in Korean)

45. Silter, G. E. (1980), “Assessment of Empirical Concrete Impact Formulas,” *Journal of the Structural Division*, ASCE, V. 106, No. 5, 1023-1045.

46. Stevenson, J. D. (2006), “Code for Concrete Reactor Vessels and Containments,” *Companion Guide to the ASME Boiler & Pressure Vessel Code, Volume 1, Second Edition*, ASME Press, 437-457.

47. Sugano, T., Tsubota, H., Kasai, Y., Koshika, N., Ohnuma, H., Riesemann, W. A., Bickel, D. C., and Parks, M. B. (1993a), “Local Damage to Reinforced Concrete Structures Caused by Impact of Aircraft Engine Missiles Part 1. Test Program, Method and Results,” *Nuclear Engineering and Design*, V. 140, 387-405.

48. Sugano, T., Tsubota, H., Kasai, Y., Koshika, N., Ohnuma, H., Riesemann, W. A., Bickel, D. C., and Parks, M. B. (1993b), “Local Damage to Reinforced Concrete Structures Caused by Impact of Aircraft Engine Missiles Part 2. Test Program, Method and Results,” *Nuclear Engineering and Design*, V. 140, 387-405.

49. Sugano, T., Tsubota, H., Kasai, Y., Koshika, N., Orui, S., Von Riesemann, W.

A., Bickel, D. D., and Parks, M. B. (1993c), “Full-Scale Aircraft Impact Test for Evaluation of Impact Force,” *Nuclear Engineering and Design*, V. 140, No. 3, 373-385.

50. Tavarez, F. A., Bank, L. C., and Plesha, M.E. (2003), “Analysis of Fiber-Reinforced Polymer Composite Grid Reinforced Concrete Beams,” *ACI Structural Journal*, V. 100, NO. 2, 250-258.

51. The Nuclear Energy Institute (NEI) (2009), Methodology for Performing Aircraft Impact Assessments for New Plant Designs, NEI 07-13, NEI, Washington, DC, U.S.A.

52. The Nuclear Energy Institute (NEI) (2011), Methodology for Performing Aircraft Impact Assessments for New Plant Designs, NEI 07-13 Revision 8P, Washington, DC, U.S.A.

53. Vasudevan, A. K. (2012), Finite Element Analysis and Experimental Comparison of Doubly Reinforced Concrete Slabs Subjected to Blast Loads, Master’s Thesis, Department of Civil Engineering, University of Missouri-Kansas City, Kansas City, MO, U.S.A.

54. Wilt, T., Chowdhury, A., and Cox, P. A. (2011), “Response of Reinforced Concrete Structures to Aircraft Crash Impact,” Prepared for U.S. Nuclear Regulatory Commission Contract NRC-02-07-006.

55. Wu, Y., Crawford, J. E., Magallances, J. M. (2012), “Performance of LS-DYNA Concrete Constitutive Models”, *12th International LS-DYNA Users Conference*, Detroit, MI, U.S.A.

56. Yoon, E.-S., Baik, Y.-K., and Park, S.-H. (2009), “Evaluation of the Compressive Strength of Concrete of Reactor Containment Building in Shinwolsong Unit 1 and 2 NPP,” *Transactions of the Korean Nuclear Society Spring Meeting*, Jeju, Korea.

Appendix A : Keywords for F-4D Jet Impact

```
*KEYWORD

*CONTROL_CONTACT
$#   slsfac     rwpnal     islchk     shlthk     penopt     thkchg      orien     enmass
       0.0        0.0          1          0          0          0          1          0
$#   usrstr     usrfrc     nsbcs     interm      xpene      ssthk      ecdt    tiedprj
         0          0          0          0        0.0          0          0          0
$#    sfric      dfric        edc        vfc         th      th_sf     pen_sf
       0.0        0.0        0.0        0.0        0.0        0.0        0.0
$#   ignore     frceng    skiprwg     outseg    spotstp    spotdel    spothin
         0          0          0          0          0          0        0.0
$#     isym     nserod     rwgaps     rwgdth      rwksf       icov     swradf     ithoff
         0          0          1        0.0        1.0          0        0.0          0
$#   shledg     pstiff     ithcnt     tdcnof      ftall     unused     shltrw
         0          0          0          0          0                    0.0

*CONTROL_DAMPING
$#   nrcyck      drtol      drfctr      drterm      tssfdr      irelal      edttl     idrflg
         0        0.0        0.0        0.0        0.0           0        0.0          0

*CONTROL_ENERGY
$#      hgen       rwen      slnten       rylen
          2          2          2          2
*CONTROL_SPH
$#      ncbs      boxid         dt       idim     memory       form      start       maxv
          1  01.00000E20          0        150          0          0  0.01.00000E15
$#      cont      deriv        ini      ishow      ierod      icont      iavis      isymp
          0          0          0          0          0          0          0        100

*CONTROL_STRUCTURED

*CONTROL_TERMINATION
$#   endtim     endcyc      dtmin     endeng     endmas
       0.1          0        0.0  0.01.000000E8

*CONTROL_TIMESTEP
$#   dtinit     tssfac       isdo     tslimt      dt2ms       lctm      erode       ms1st
       0.0        0.5          0        0.0        0.0          0          0          0
$#   dt2msf    dt2mslc      imscl     unused     unused      rmscl
       0.0          0          0                             0.0

*DATABASE_GLSTAT
$#         dt     binary       lcur      ioopt
2.00000E-4            0          0          1

*DATABASE_MATSUM
$#         dt     binary       lcur      ioopt
2.00000E-4            0          0          1

*DATABASE_NODOUT
$#         dt     binary       lcur      ioopt    option1    option2
```

```
2.00000E-4          0          0          1        0.0          0

*DATABASE_RCFORC
$#        dt     binary       lcur      ioopt
2.00000E-4          0          0          1

*DATABASE_RWFORC
$#        dt     binary       lcur      ioopt
2.00000E-4          0          0          1

*DATABASE_SPHOUT
$#        dt     binary       lcur      ioopt
2.00000E-4          0          0          1

*DATABASE_BINARY_D3PLOT
$#        dt       lcdt       beam      npltc     psetid
2.00000E-4          0          0          0          0
$#     ioopt
           0

*DATABASE_EXTENT_BINARY
$#     neiph      neips     maxint     strflg     sigflg     epsflg     rltflg     engflg
           0          0          0          0          1          1          1          1
$#   cmpflg     ieverp     beamip      dcomp      shge       stssz      n3thdt     ialemat
           0          0          0          1          1          1          2          0
$# nintsld     pkp_sen       sclp      hydro      msscl      therm      intout     nodout
           0          0        1.0          0          0       0ALL        ALL
$#      dtdt     resplt
           0          0

*DATABASE_HISTORY_NODE
$#       id1        id2        id3        id4        id5        id6        id7        id8
    288485     540076     288442      79718     288528          0          0
0

*BOUNDARY_SPC_SET
$#      nsid        cid       dofx       dofy       dofz      dofrx      dofry      dofrz
           2          0          1          0          1          1          1          1

*SET_NODE_LIST_TITLE
NODESET(SPC) 2
$#       sid        da1        da2        da3        da4     solver
           2        0.0        0.0        0.0       0.0MECH
$#      nid1       nid2       nid3       nid4       nid5       nid6       nid7       nid8
     42197      42198      42199      42200      42201      42202      42203      42204
……
……
……

*CONTACT_AUTOMATIC_NODES_TO_SURFACE
$#       cid                                                                   title
```

```
$#     ssid       msid       sstyp      mstyp      sboxid     mboxid       spr        mpr
         1          2          4          2          0          0          0          0
$#       fs         fd         dc         vc        vdc    penchk         bt         dt
       0.0        0.0        0.0        0.0        0.0          0        0.0        0.0
$#      sfs        sfm        sst        mst       sfst       sfmt        fsf        vsf
       0.0        0.0       0.01        0.0        0.0        0.0        0.0        0.0
$#     soft     sofscl     lcidab     maxpar      sbopt      depth      bsort     frcfrq
         1        0.1          0        0.0        0.0          0          0          0

*SET_NODE_LIST_TITLE
Aircraft
$#      sid        da1        da2        da3        da4     solver
         1        0.0        0.0        0.0       0.0MECH
$#     nid1       nid2       nid3       nid4       nid5       nid6       nid7       nid8
         1          2          3          4          5          6          7          8
……
……
……

*SET_PART_LIST_TITLE
Target
$#      sid        da1        da2        da3        da4     solver
         2        0.0        0.0        0.0       0.0MECH
$#     pid1       pid2       pid3       pid4       pid5       pid6       pid7       pid8
         1          2          0          0          0          0          0          0

*PART
$#                                                                             title
Concrete
$#      pid      secid        mid      eosid       hgid       grav     adpopt       tmid
         1          1          1          0          1          0          0          0

*SECTION_SOLID_TITLE
Concrete
$#    secid     elform        aet
         1          1          0

*MAT_CSCM_CONCRETE_TITLE
Concrete
$#      mid         ro      nplot      incre      irate      erode      recov    itretrc
         1     2615.0          1        0.0          0       1.05       10.0          0
$#     pred
       0.0
$#      fpc       dagg      units
3.000000E7      0.019          4

*HOURGLASS
$#     hgid        ihq         qm        ibq         q1         q2     qb/vdc         qw
         1          5      0.001          0        1.5       0.06        0.1        0.1

*PART
```

```
$#                                                                  title
Steel
$#     pid     secid       mid     eosid      hgid      grav    adpopt      tmid
         2         2         2         0         1         0         0         0

*SECTION_BEAM_TITLE
Rebar
$#   secid    elform      shrf   qr/irid       cst     scoor       nsm
         2         3    0.8333         2         1       0.0       0.0
$#       a     rampt    stress
1.26700E-4       0.0       0.0

*MAT_PLASTIC_KINEMATIC_TITLE
Steel
$#     mid        ro         e        pr      sigy      etan      beta
         2 7850.02.00000E11      0.34.200000E8       0.0       0.0
$#     src       srp        fs        vp
       0.0       0.0       0.2       0.0

*PART
$#                                                                  title

$#     pid     secid       mid     eosid      hgid      grav    adpopt      tmid
        15       101       101         0         0         0         0         0
*SECTION_SPH_TITLE
Aircraft
$#   secid      cslh      hmin      hmax    sphini     death     start
       101       1.2       0.0       0.0       0.0       0.0       0.0

*MAT_PLASTIC_KINEMATIC_TITLE
Aircraft
$#     mid        ro         e        pr      sigy      etan      beta
       101 2770.06.90000E10      0.339.500000E7       0.0       0.0
$#     src       srp        fs        vp
       0.0       0.0       1.8       0.0

*PART
$#                                                                  title
$#     pid     secid       mid     eosid      hgid      grav    adpopt      tmid
        16       101       101         0         0         0         0         0

*PART
$#                                                                  title
$#     pid     secid       mid     eosid      hgid      grav    adpopt      tmid
        17       101       101         0         0         0         0         0

*PART
$#                                                                  title
$#     pid     secid       mid     eosid      hgid      grav    adpopt      tmid
        18       101       101         0         0         0         0         0
```

```
*PART
$#                                                                  title
$#     pid     secid       mid     eosid      hgid      grav    adpopt      tmid
        19       101       101         0         0         0         0         0

*PART
$#                                                                  title
$#     pid     secid       mid     eosid      hgid      grav    adpopt      tmid
        20       101       101         0         0         0         0         0

*PART
$#                                                                  title
$#     pid     secid       mid     eosid      hgid      grav    adpopt      tmid
        21       101       101         0         0         0         0         0

*PART
$#                                                                  title
$#     pid     secid       mid     eosid      hgid      grav    adpopt      tmid
        22       101       101         0         0         0         0         0

*PART
$#                                                                  title
$#     pid     secid       mid     eosid      hgid      grav    adpopt      tmid
        23       101       101         0         0         0         0         0

*PART
$#                                                                  title
$#     pid     secid       mid     eosid      hgid      grav    adpopt      tmid
        24       101       101         0         0         0         0         0

*PART
$#                                                                  title
$#     pid     secid       mid     eosid      hgid      grav    adpopt      tmid
        25       101       101         0         0         0         0         0

*PART
$#                                                                  title
$#     pid     secid       mid     eosid      hgid      grav    adpopt      tmid
        26       101       101         0         0         0         0         0

*PART
$#                                                                  title
$#     pid     secid       mid     eosid      hgid      grav    adpopt      tmid
        27       101       101         0         0         0         0         0

*PART
$#                                                                  title
$#     pid     secid       mid     eosid      hgid      grav    adpopt      tmid
        28       101       101         0         0         0         0         0

*PART
```

```
$#                                                                  title
$#     pid     secid       mid     eosid      hgid      grav    adpopt      tmid
        29       101       101         0         0         0         0         0

*PART
$#                                                                  title
$#     pid     secid       mid     eosid      hgid      grav    adpopt      tmid
        30       101       101         0         0         0         0         0

*PART
$#                                                                  title
$#     pid     secid       mid     eosid      hgid      grav    adpopt      tmid
        31       101       101         0         0         0         0         0

*INITIAL_VELOCITY
$#    nsid    nsidex     boxid    irigid     icid
         0         0       100         0        0
$#      vx        vy        vz       vxr       vyr       vzr
       0.0    -215.0       0.0       0.0       0.0       0.0

*DEFINE_BOX
$#   boxid       xmn       xmx       ymn       ymx       zmn       zmx
       100      -6.0       6.0       0.0      18.0      -1.0       4.0

*CONSTRAINED_LAGRANGE_IN_SOLID
$#   slave    master     sstyp     mstyp     nquad     ctype     direc     mcoup
         2         1         1         1         0         2         1         0
$#   start       end      pfac      fric    frcmin      norm   normtyp      damp
       0.0 1.00000E10       0.1       0.0       0.5         0         0       0.0
$#      cq      hmin      hmax     ileak     pleak   lcidpor     nvent  blockage
       0.0       0.0       0.0         0       0.1         0         0         0
$#  iboxid   ipenchk    intforc   ialesof    lagmul   pfacmm      thkf
         0         0         0         0       0.0         0       0.0

*ELEMENT_SOLID
$#    eid       pid        n1        n2        n3        n4        n5        n6        n7        n8
  199015         1     42197     42198     42299     42298     47550     47551     47652
47651
……
……
……

*ELEMENT_BEAM
$#    eid       pid        n1        n2        n3       rt1       rr1       rt2       rr2     local
  719015         2 131078 131179         0         0         0         0         0         2
……
……
……

*ELEMENT_SPH
$#    nid       pid              mass
```

```
         1        15          0.222222
……
……
……

*NODE
$#     nid               x               y               z      tc      rc
         1     -0.300003             0.5        0.022296       0       0
         2     -0.300003             0.5        0.122296       0       0
……
……
……

*END
```

Appendix B : Keywords for Blade Impact

```
*KEYWORD

*CONTROL_ACCURACY
$#      osu       inn    pidosu      iacc
         0         3         0         0

*CONTROL_ENERGY
$#     hgen      rwen     slnten     rylen
         2         2         2         2

*CONTROL_HOURGLASS
$#      ihq        qh
         3      0.05

*CONTROL_SOLUTION
$#     soln       nlq     isnan     lcint
         0         0         1       100

*CONTROL_TERMINATION
$#   endtim    endcyc     dtmin    endeng    endmas
      0.01         0       0.0   0.01.000000E8

*CONTROL_TIMESTEP
$#   dtinit    tssfac      isdo    tslimt     dt2ms      lctm     erode      ms1st
       0.0       0.9         0       0.0       0.0         0         0          0
$#   dt2msf   dt2mslc     imscl    unused    unused     rmscl
       0.0         0         0                         0.0

*DATABASE_GLSTAT
$#        dt    binary      lcur     ioopt
5.00000E-5         1         0         1

*DATABASE_MATSUM
$#        dt    binary      lcur     ioopt
5.00000E-5         1         0         1

*DATABASE_BINARY_D3PLOT
$#        dt      lcdt      beam     npltc    psetid
5.00000E-5         0         0         0         0
$#     ioopt
         0

*BOUNDARY_SPC_SET
$#     nsid       cid      dofx      dofy      dofz     dofrx     dofry     dofrz
         1         0         1         1         1         1         1         1

*SET_NODE_LIST_TITLE
NODESET(SPC) 1
$#      sid       da1       da2       da3       da4    solver
         1       0.0       0.0       0.0     0.0MECH
$#     nid1      nid2      nid3      nid4      nid5      nid6      nid7      nid8
```

```
    2673       2674       2675       2676       2677       2678       2679       2680
……
……
……

*CONTACT_AUTOMATIC_SURFACE_TO_SURFACE
$#      cid                                                                 title
$#     ssid       msid      sstyp      mstyp     sboxid     mboxid       spr        mpr
         30          1          3          0          0          0          0          0
$#       fs         fd         dc         vc        vdc    penchk         bt         dt
        0.0        0.0        0.0        0.0        0.0          0  0.01.00000E20
$#      sfs        sfm        sst        mst       sfst       sfmt        fsf        vsf
        1.0        1.0        0.0        0.0        1.0        1.0        1.0        1.0

*SET_SEGMENT_TITLE
surface
$#      sid        da1        da2        da3        da4     solver
          1        0.0        0.0        0.0        0.0MECH
$#       n1         n2         n3         n4         a1         a2         a3         a4
    196380     196379     196352     196353        0.0        0.0        0.0
0.0
……
……
……

*CONTACT_AUTOMATIC_NODES_TO_SURFACE
$#      cid                                                                 title
$#     ssid       msid      sstyp      mstyp     sboxid     mboxid       spr        mpr
          2         30          2          3          0          0          0          0
$#       fs         fd         dc         vc        vdc    penchk         bt         dt
        0.0        0.0        0.0        0.0        0.0          0  0.01.00000E20
$#      sfs        sfm        sst        mst       sfst       sfmt        fsf        vsf
        1.0        1.0        0.0        0.0        1.0        1.0        1.0        1.0

*SET_PART_LIST_TITLE
rebar
$#      sid        da1        da2        da3        da4     solver
          2        0.0        0.0        0.0        0.0MECH
$#     pid1       pid2       pid3       pid4       pid5       pid6       pid7       pid8
         11         12         13         14         15         16          0          0

*PART
$#                                                                      title
Concrete
$#      pid      secid        mid      eosid       hgid       grav     adpopt       tmid
          2          1          1          0          0          0          0          0

*SECTION_SOLID_TITLE
concrete
$HMNAME PROPS          1Concrete
$#    secid     elform        aet
```

```
         1         1         0

*MAT_CSCM_CONCRETE_TITLE
concrete
$#     mid        ro     nplot     incre     irate     erode     recov    itretrc
         1    2400.0         1       0.0         0      1.05      10.0         0
$#    pred
       0.0
$#     fpc      dagg     units
5.080000E7      0.02         4

*PART
$#                                                                         title
REBAR#11_Floor
$#     pid     secid       mid     eosid      hgid      grav    adpopt      tmid
        11        11         2         0         0         0         0         0

*SECTION_BEAM_TITLE
#11_Floor
$#   secid    elform      shrf   qr/irid       cst     scoor       nsm
        11         3     0.833         2         1       0.0       0.0
$#       a     rampt    stress
     0.001       0.0       0.0

*MAT_PLASTIC_KINEMATIC_TITLE
steel
$#     mid        ro         e        pr      sigy      etan      beta
         2  7850.02.00000E11      0.34.200000E8       0.0       0.0
$#     src       srp        fs        vp
       0.0       0.0       0.1       0.0

*PART
$#                                                                         title
REBAR#11
$#     pid     secid       mid     eosid      hgid      grav    adpopt      tmid
        12        12         2         0         0         0         0         0

*SECTION_BEAM_TITLE
#11
$#   secid    elform      shrf   qr/irid       cst     scoor       nsm
        12         3     0.833         2         1       0.0       0.0
$#       a     rampt    stress
     0.001       0.0       0.0

*PART
$#                                                                         title
Rebar#14_130X160
$#     pid     secid       mid     eosid      hgid      grav    adpopt      tmid
        13        13         2         0         0         0         0         0

*SECTION_BEAM_TITLE
```

```
#14_130X160
$#    secid     elform      shrf   qr/irid       cst     scoor       nsm
        13          3     0.833         2         1       0.0       0.0
$#       a      rampt     stress
    0.0015        0.0        0.0

*PART
$#                                                                 title
Rebar#14_110X160
$#     pid      secid        mid     eosid      hgid      grav    adpopt      tmid
        14         14          2         0         0         0         0         0

*SECTION_BEAM_TITLE
#14_110X160
$#    secid     elform      shrf   qr/irid       cst     scoor       nsm
        14          3     0.833         2         1       0.0       0.0
$#       a      rampt     stress
    0.0015        0.0        0.0

*PART
$#                                                                 title
Rebar#14_220X160
$#     pid      secid        mid     eosid      hgid      grav    adpopt      tmid
        15         15          2         0         0         0         0         0

*SECTION_BEAM_TITLE
#14_220X160
$#    secid     elform      shrf   qr/irid       cst     scoor       nsm
        15          3     0.833         2         1       0.0       0.0
$#       a      rampt     stress
    0.0015        0.0        0.0

*PART
$#                                                                 title
Rebar#14_EW
$#     pid      secid        mid     eosid      hgid      grav    adpopt      tmid
        16         16          2         0         0         0         0         0

*SECTION_BEAM_TITLE
#14_EW
$#    secid     elform      shrf   qr/irid       cst     scoor       nsm
        16          3     0.833         2         1       0.0       0.0
$#       a      rampt     stress
   0.00435        0.0        0.0

*PART
$#                                                                 title
blade
$#     pid      secid        mid     eosid      hgid      grav    adpopt      tmid
        30         30         50         0         0         0         0         0
```

```
*SECTION_SOLID_TITLE
blade
$#    secid    elform       aet
         30          1          0

*MAT_ELASTIC_TITLE
blade
$#       mid          ro           e          pr          da          db  not used
         50     1700.02.46000E10         0.3         0.0         0.0           0

*INITIAL_VELOCITY_NODE
$#       nid          vx          vy          vz         vxr         vyr         vzr        icid
   2452455         0.0      -100.0         0.0         0.0         0.0         0.0           0
……
……
……

*CONSTRAINED_LAGRANGE_IN_SOLID_TITLE
$#   coupid                                                                 title
          1concrete-rebar
$#    slave    master     sstyp     mstyp     nquad     ctype     direc     mcoup
          2         2         0         1         0         2         1         0
$#    start       end      pfac      fric    frcmin      norm   normtyp      damp
        0.01.00000E10       0.1       0.0       0.5         0         0       0.0
$#       cq      hmin      hmax     ileak     pleak   lcidpor     nvent  blockage
        0.0       0.0       0.0         0       0.1         0         0         0
$#   iboxid   ipenchk   intforc   ialesof    lagmul    pfacmm      thkf
          0         0         0         0       0.0         0       0.0

*ELEMENT_SOLID
$#    eid     pid      n1      n2      n3      n4      n5      n6      n7      n8
        1       2    2918   50429  298969   50413       1    2857   50301
2886
……
……
……

*ELEMENT_BEAM
$#    eid     pid      n1      n2      n3     rt1     rr1     rt2     rr2   local
  921433      12 1276324 1277024       0       0       0       0       0
2
……
……
……

*NODE
$#    nid               x               y               z      tc      rc
        1           1.524         33.8328         43.1292       0       0
……

*END
```

국 문 초 록

LS-DYNA 프로그램을 이용한 콘크리트 구조물의 비상체 충돌에 관한 수치해석 연구

콘크리트는 장대교량과 같은 토목공사부터 초고층 건축물과 같은 건축공사에 이르기까지 광범위하게 사용되어 온 재료이다. 콘크리트는 이와 같은 전형적인 구조물뿐만 아니라, 원전 구조물과 같은 국가중요시설에서도 그 기능을 다하기 위해 다양한 방법으로 사용되어 왔다.

본 논문은 유한요소해석 프로그램을 이용하여 콘크리트 목표물에 가해지는 비상체 충돌에 관한 연구를 수행함으로써 다양한 충돌 해석에 관하여 해석적 방법을 제시하는데 그 목적이 있다. 이를 위해 1988 년 미국 Sandia National Laboratories(SNL)에서 수행한 전투기 충돌 실험에 대하여 유한요소해석 프로그램을 활용한 수치해석을 수행하였다. 아울러, 이 연구에서는 원자력 발전소의 보조건물에 풍력발전 블레이드 파편이 충돌하는 가상 시나리오에 대한 해석도 다루었다.

유한요소해석은 실증실험과 비교하면 시간과 비용이 크게 절감되는 장점이 있다. 그리고 해석모델은 실제 실험을 수행할 경우 고려되는 시간, 장소, 실험체의 크기에 구애받지 않고 충돌현상을 효과적으로 예측하는 데 있어 매우 중요하다. 따라서 본 연구에서 충돌과 콘크리트의 국부파괴를 예측하기 위해 제시된 해석적 방법은 국가시설이나 방호시설에 관한 연구뿐만 아니라, 향후 이와 유사한 충돌관련 연구에서 적극적으로 활용될 수 있을 것으로 사료된다.

핵심용어: 항공기 충돌, 비상체 충돌, 콘크리트 구조물, 국부파괴, 유한요소해석

학번: 2016-21093